Ricerca Sistema Elettrico	Sigla di identificazione	Distrib.	Pag.	di
	ADPFISS – LP2 – 057	L	1	48

Titolo

Numerical analysis Flow Blockage phenomena in the ALFRED FA: preliminary study on neutronic feedback

Descrittori

Tipologia del documento:

Collocazione contrattuale: Accordo di programma ENEA-MSE su sicurezza nucleare e reattori di IV generazione

Argomenti trattati:

Generation IV reactors, Tecnologia dei metalli liquidi, Termoidraulica dei reattori nucleari

Sommario

In the context of GEN-IV Heavy Liquid Metal safety studies, the flow blockage in a Fuel sub-assembly is considered one of the main issues to be addressed and the most important and realistic accident for LFR Fuel Assembly. The present document is a first step towards a detailed analysis of such phenomena, and a CFD model and approach is presented to have a detailed thermo-fluid dynamic picture in the case of blockage. In particular, the internal flow blockage in the ALFRED hexagonal wrapped Fuel Assembly is presented here. At this stage, a conservative analysis has been carried out basing on the main geometrical and physical features. In the first part of the work, reactivity feedback, as well as axial power profile, was not considered. Nevertheless, relevant indications derives from the analysis of the results. Results indicate that critical conditions, with clad temperatures around ~900°C, are reached with blockage larger than 30% in terms of area fraction. Transient analyses with fully resolved SST-ω turbulence model were also carried out. In the second part of the work, a first evaluation of the neutronic feedback is given. The quantification is performed by a one-way coupling of the neutronic deterministic code ERANOS and the CFD code CFX. Results indicates that the influence of the neutronic feedback on the power is around 10% and therefore a preliminary safety evaluation provides results which support current fuel assembly design.

Note:

Autori: I. DI PIAZZA, P. CONSOLE CAMPRINI (ENEA)

Copia n. **In carico a:**

REV.	DESCRIZIONE	DATA		REDAZIONE	CONVALIDA	APPROVAZIONE
2			NOME			
			FIRMA			
1			NOME			
			FIRMA			
0	EMISSIONE	19/09/2014	NOME	I.Di Piazza	A. Del Nevo	M. Tarantino
			FIRMA			

Index

1. Introduction

The flow blockage accident in a Fuel Assembly (FA) of a nuclear reactor consists of a partial or total occlusion of the flow passage area. This leads in general to a degradation of the heat transfer between the FA and the coolant potentially causing a temperature peak in the clad which can eventually lead to the fusion of the clad itself. While a partial blockage at the fuel assembly foot may be dangerous for the integrity of the FA (e.g. Fermi 1 fuel meltdown accident), see NRC (2011) and Bertini (1980), the phenomena can be investigated and assessed by an integral system code in order to devise proper mitigation actions. On the other hand, an internal blockage can be even more dangerous and it is not easy to detect; this kind of blockage can be more effectively modeled and studied by a proper use of a CFD code.

Regarding the sodium fast reactors, they generally adopt wire-spaced bundles, and the accumulation of debris from failed fuel pins or broken wires, generally occurs *along* the wire. Therefore, in this case, the preferential shape of the blockage is elongated and it follows the helicoid wire (Schultheiss, 1987).

For grid-spaced fuel assemblies, experimental results on blockage growth by particles show that particles with sizes spread around the subchannel dimensions are collected at the spacer grid. A horizontal *plate like* particle bed with strong radial growth tendency was found (Schultheiss, 1987). In this paper the attention is focused on the grid-spaced bundles. From these remarks, the most likely internal blockage in a grid-spaced bundle is at the lower spacer grid, and, if the spacer grid is positioned in the active region, a remarkable effect can be evidenced and a possible damage can occur. In principle, in the latter case, two different effects can be distinguished:

- ✓ A *local* effect due to the stagnation-recirculation/wake region downstream of the blockage, with a local minimum of the heat transfer and a clad temperature peak;
- ✓ A *global* effect due to the lower mass flow rate in the blocked subchannels; this effect leads to an increase of the bulk fluid temperature with respect to the ‘unblocked’ regions and a consequent peak in the clad temperature at the end of the active region.

In Figure 1, a very conceptual representation of the flow blockage accident is shown. The flow passes the obstacle and a recirculation region with relatively low velocities ensues just downstream of the blockage. This flow pattern leads to the phenomenology described above as a local effect and a global effect.

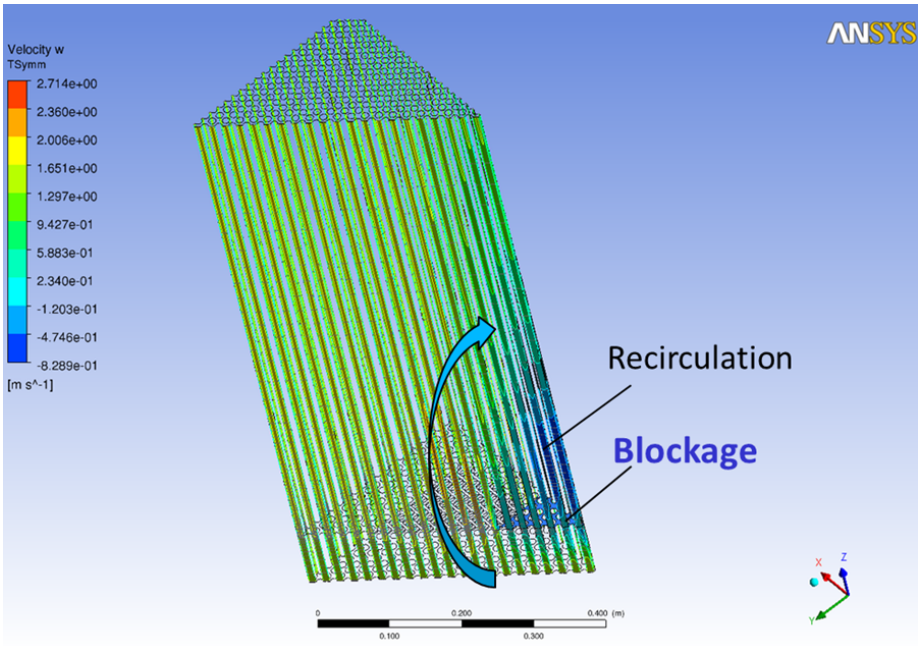

Figure 1 Schematic representation of a flow blockage.

As a consequence of the above considerations, the most critical (and conservative) case to be considered from the safety point of view is the blockage at the beginning of the active zone, where the local effect is present, and the global effect is maximum because the entire active length is available to heat up the bulk temperature of the coolant in the blocked subchannels.

In this report, numerical analysis will be presented of flow blockage event in a fuel assembly of Heavy Liquid Metal (Lead) cooled ALFRED reactor. Due to the crucial role of the heat transfer in the stagnation-recirculation/wake region in this context, the turbulence in this region must be carefully assessed. In fact, in the case where the turbulence thermal diffusion overcomes the molecular diffusion, the clad temperature peak downstream the blockage is largely independent of the nature of the fluid, i.e. by the Prandtl number. On the opposite, if the recirculation region is a 'stagnation' region with low turbulent heat transfer, the physical nature of the coolant, and in particular the Prandtl number, plays the major role in the establishment of the peak temperature. From the literature, it is not very clear which of the two phenomena is the most important, although some simplified theories assume that the turbulence dominates downstream the blockage and therefore the temperature peak is independent by the Reynolds and the Prandtl number (Han & Fontana (1977)). Probably, a systematic comparison between different coolants has not yet been performed; therefore any preliminary conclusions may not have sufficient basis.

In any case, in References, the specific literature for flow blockage *in liquid metal cooled bundles* were reported, i.e. sodium and lead, being the flow blockage phenomena in light water reactors a quite different matter because of the unity order of the Prandtl number (Chang et al (2011), Han and Fontana (1977), Hooper and Wood (1982), Klein and Sesonske (1981), Kirsch (1975), Lu et al. (2009)).

For the heavy liquid metal cooled GEN-IV reactors studied in these years by the scientific community, the flow blockage accident must be considered as one of the reference accidents, and probably the most dangerous for the core integrity. In fact, most of the known accident that have occurred in the LBE cooled fast reactors of the Alpha-class Russian nuclear submarines, are apparently caused by a flow blockage accident, see Zrodnikov et al. (2000), Warden et al. (1997).

An interesting review on flow blockage phenomena in LMFBR fuel assemblies is given in Han & Fontana (1977). The paper gives a quite complete review of the investigations on flow blockage in sodium reactors and keeps into account all the technical and scientific development of '60s and '70s on sodium cooled fast reactors. The review especially refers to experimental and analytical investigations performed in United States and Germany, the authors develop an analytical approach to predict the flow blockage effects.

The blockages at the foot of a fuel assembly may have significant effects in the fuel assembly if coolant mass flow rate is significantly reduced and the blockages would be easily detectable in the case of closed FA . The effect of blockage on reactor safety depends in principle on several factors: size and location of the blockage, nature of the coolant, fuel pin power, and coolant velocity in the assembly. In closed FA, blockages in flow channels will increase the hydraulic resistance and reduce the flow rate.

Experimental data on Clinch River Breeder Reactor (CRBR), the Fast-Flux test facility (FFTF), and the German Sodium-cooled fast Reactor (SNR) are provided in the review. CRBR and FFTF have 217 fuel pins each assembly and are wire-wrapped spaced, while SNR FA consists of 169 pins in a triangular lattice, grid-spaced, and enclosed in a hexagonal wrap. The SNR is particularly interesting for our purposes, because the reference configuration for a Lead Fast Reactor Demonstrator is grid-spaced.

With the typical approach of the '70s, Kirsch (1974) developed a simplified theory to describe the thermo-fluid dynamic phenomena downstream the blockage. The basic assumption is that turbulent diffusion dominates both for momentum and for energy, and thus the molecular heat transfer is negligible. With this hypothesis, the author shows that for sufficiently high Reynolds and Peclet numbers, the dimensionless temperature distribution in the wake is independent of the Reynolds and the Prandtl number, i.e. by the flow and the nature of the fluid. Comparison between experimental results in sodium and water seems to partially confirm these conclusions with a difference between the two fluids of 25%. This difference is probably due to the residual influence of the coolant. Therefore, according to the author, it could be possible to have a 'universal' *dimensionless* temperature profile function of the fraction β of the blocked flow area. From this point of view, the main difference between sodium and lead as coolant is the possible onset of boiling in sodium due to the lower boiling temperature (890 °C) with positive reactivity feedback and power excursion. In lead, with a boiling temperature of 1740 °C, this scenario is unlikely in the case of flow blockage.

From a theoretical point of view, it could be interesting to confirm or disconfirm these conclusions by CFD numerical simulations, i.e. by the direct solution of the Navier-Stokes equations. The only way to numerically investigate the flow blockage in realistic configurations is by the use of turbulence models, being DNS or LES not feasible at Reynolds numbers ~10^5 typical of the fuel assemblies. The

controversial point is the ability of the turbulence models to describe the turbulent heat transfer for liquid metals, but probably this issue was too much emphasized in the last years, and the same turbulence models developed for unity Prandtl number fluids like 'water' can be largely used to compute turbulent heat transfer in low Prandtl number fluids with the same level of accuracy as in water. Moreover, the velocity fluctuations have the same nature in all the fluids, and thus the turbulence level in the wake region can be predicted for liquid metals with the same accuracy as in water. This latter prejudice justifies further theoretical studies in support of experimental results in the '80s (Klein and Sesonske (1981), Hooper and Wood (1982)), when computational tools had already been available. Not so many CFD studies appeared in the 90's and 00' on the flow blockage in Liquid Metal cooled fast reactors, probably because of the decreasing importance of these kinds of reactors.
In the last years, due to the growing interest in the developing of GEN-IV prototypes and Demonstrators, the interest in sodium-cooled and lead-cooled bundles is high again. Nevertheless, only a small number of CFD studies appeared in the literature and sometimes these studies adopted simplified models for the bundle (porous media) and the focus was on the whole reactor (Maity et al. (2011)). Generally, system codes like RELAP are commonly adopted by the safety analysts to compute flow blockage in reactor Fuel Assemblies (Lu et al. (2009)), although the local nature of the involved phenomena does not fully justify this common practice. An intermediate practices is to apply subchannels codes to evaluate these phenomena, see e.g. Chang et al. (2011) for SFR.

In the first part of the present work (Sections 2 and 3), the main results related to the pure thermo-fluid dynamic analysis of the flow blockage in the ALFRED FA will be presented. This analysis does not include the neutronic feedback due to the local and overall FA temperature variation induced by the blockage. At a first step, this feedback was considered a second order effect, and the results were published in International journal (Di Piazza et al.(2014)).

Section 4 is devoted to a preliminary quantification of the neutronic feedback effect on the power and on the temperature field. The methodology will be described in details in Section 4, and it is based on an evaluation of the feedback coefficients via the ERANOS 2.1 neutronic code (G. Rimpault, (2002)). These coefficients are used to quantify the reactivity insertion due to the thermal transient obtained by a CFD code. The effect of reactivity insertion on the power is then evaluated by the implementation of the 6-groups point kinetic equations into the CFX code. This scheme opens the possibility of a future two-way coupling between codes.
According to the literature, flow blockage accident simulations were performed by means of different methods and neutronic feedback are thus considered following each related assumption and hypothesis.
Actual temperature fields throughout the core – namely inside fuel, cladding and coolant – are subjected to transients and such modifications induce global multiplication coefficient of the system to vary. As a consequence, related positive or negative reactivity insertion occurs.
Moreover, fuel temperature change has an impact on neutron absorption via Doppler broadening acting on resonance self-shielding. By contrast, materials density is worth to be considered as well. In particular, coolant is mainly concerned since temperature increase impacts absorption and reflection features – namely neutron balance of the core as a whole.

LFRs are fast-spectrum systems in which flux shape is normally treated according to transport theory as for small nuclear systems - compared to typical diffusion length.
Thus, preliminary assessment is worth to be carried out regarding neutron kinetics method employed - best trade-off between results precision and calculation strategy needs is achieved.

Literature review pointed out several flow blockage studies performed through neutron point kinetics approximation.
Foremost, material testing reactor cores are treated in this fashion to simulate either partial or full channel blockage and related transients (Qing Lu et al. (2009)). The latter paper accounts for constant power profile according to such a kinetics model, coherently to other studies for IAEA standard MTR (Adorni et al. (2005)).
Concerning water-cooled reactors at large, it is worth to underline how flow blockage analysis is in principle considered as a thermal-hydraulic issue in which many studies mainly concern temperature field analysis even with loosely-coupled neutronic models (X. J. Liu (2013)). 3D coupling efforts are anyway still present in transport approximation for some local detailed analyses (S. Jewer (2014)).
Similarly, preliminary references show flow blockage evaluations being small amounts of reactivity concerned by central channel void or blockage as in Salah Ud-Din Khan et al. (2014) or as reported by Hyung Min Son et al. (2015).
Local central-channel effects are treated also by means of a particular weighted feedback coefficient utilization. Total core parameters are split according to neutron importance (adjoint flux) regarding a particular part of reactor domain. This appears a good compromise in utilizing integral information and local investigation needs (Ampomah-Amoako (2013)).
Flow blockage accidents are conversely considered in case of sodium-cooled reactors and a study is reported in Chang et al. (2011). A channel analysis is performed by a channel blockage and neutronic feedback is related to total core point kinetics.
Present study aims at improving previous evaluations by means of neutronic feedback for a detailed flow blockage accident analysis - related impact on temperature is computed by means of a one-way coupling model. Very few examples are treated in literature concerning LFRs blockage accident simulations and it appears a quite cutting-edge topic to authors' knowledge.
Neutron point kinetics is then retained as a modelling approach. Feedback coefficients are evaluated through local properties variations and related impact on global system reactivity.
Actual reactivity insertion and variation is then applied to the whole system in a point kinetics approximation in which local previous results are employed in a lumped system model.
First design verification is coherent with simulation hypothesis, point kinetics is provided by local information effectively related to system change during flow blockage transients.

2. Numerical Models and methods

2.1. General Considerations

From the arguments in section 1, it is evident that the flow blockage is basically a local phenomenon, and the main issue to investigate is the thermal-hydraulic behaviour of the region downstream of the obstacle because it determines the clad temperature peak. For this reason, a local fully detailed CFD

analysis was carried out in order to assess the impacts of a flow blockage. The viscous sub-layer was resolved with several points in all the simulations presented here. A value of y^+~1 is guaranteed in the whole domain.

From a physical point of view, the reactivity feedback due to the temperature variation in the domain was not considered at this stage in Section 2 and 3. A constant power distribution was considered as well, neglecting the axial power profile typical of the nuclear reactors. In addition, spacer grids have not been modelled being not very relevant for the phenomena to investigate.

The computational domain includes the active region, the non-active region upstream and downstream and the FA plenum. The wrap of the FA is modelled as well and a bypass flow is considered; the thermal conduction in the pin clad is kept into account.

Constant thermo-physical properties were assumed for Lead at 450°C, according to **Table 1**(OECD, 2007). For the clad material (SS 15-15 Ti) and the wrap material (T91), constant physical properties were considered at 450 °C according to **Table 2** and **Table 3** (RCC-MRx, 2010).

Table 1 Physical properties of Lead at 450 °C.

$\rho\,[kg/m^3]$	Density	10503
$\nu\,[m^2/s]$	Kinematic viscosity	$1.9\cdot10^{-7}$
$k\,[W/mK]$	Thermal Conductivity	17.15
$c_p\,[J/kgK]$	Specific heat at constant pressure	145.9
Pr	Prandtl number	0.01697
$\alpha\,[1/K]$	Thermal expansion coefficient	$1.137\cdot10^{-4}$

Table 2 Physical properties of SS 15-15 Ti (Clad material) at 450 °C.

$\rho\,[kg/m^3]$	Density	7800
$k\,[W/mK]$	Thermal Conductivity	20.2
$c_p\,[J/kgK]$	Specific heat at constant pressure	565

Table 3 Physical properties of T91 (Wrap material) at 450 °C.

$\rho\,[kg/m^3]$	Density	7600
$k\,[W/mK]$	Thermal Conductivity	28.3
$c_p\,[J/kgK]$	Specific heat at constant pressure	600

The buoyancy term was explicitly included in the momentum equation, due to the potential role of the local buoyancy in promoting heat transfer in the wake region. The exact production term in the kinetic energy equation was included as well. Fully convergence was reached in all the simulations presented in this paper.

2.2. Numerical Methods

The general purpose code ANSYS CFX 13 was used for all the numerical simulations presented in this paper. The code employs a coupled technique, which simultaneously solves all the transport equations in the whole domain through a false time-step algorithm. The linearized system of equations is preconditioned in order to reduce all the eigenvalues to the same order of magnitude. The multi-grid approach reduces the low frequency error, converting it to a high frequency error at the finest grid level; this results in a great acceleration of convergence. Although, with this method, a single iteration is slower than a single iteration in the classical decoupled (segregated) SIMPLE approach, the number of iterations necessary for a full convergence to a steady state is generally of the order of 10^2, against typical values of 10^3 for decoupled algorithms. For the transient calculation, the CFL=1 criterion was adopted leading to a time step ~ 1 *ms*.

2.3. Turbulence Models

The SST (Shear Stress Transport) k-ω model by Menter (1994) is extensively used in this paper. It is formulated to solve the viscous sub-layer explicitly, and requires several computational grid points inside this latter. The model applies the k-ω model close to the wall, and the k-ε model (in a k-ω formulation) in the core region, with a blending function in between. It was originally designed to provide accurate predictions of flow separation under adverse pressure gradients, but it was applied to a large variety of turbulent flows and is now the default and most commonly used model in CFX-13 and other CFD codes. This structural feature of the model to predict in a good way flow separation and recirculation gives a good confidence in applying the model to compute flow blockage in fuel subassemblies. The turbulent Prandtl number in the case of lead was fixed to 1.1, according to the suggestion of the literature (Cheng and Tak (2006)) and to the author's experience (Scarpa (2013)).

3. Flow Blockage in the hexagonal wrapped ALFRED FA (no reactivity feedback)

3.1. ALFRED FA CFD Model

The Fuel Assembly of the ALFRED Lead cooled reactor was considered here as the reference configuration to investigate. The fuel assembly is a wrapped hexagonal lattice bundle with 127 rods, grid-spaced, with rod diameter d=10.5 *mm*, pitch to diameter ratio p/d=1.32 and an active length L=0.6 *m*. The total thermal power of the reactor is Q~300 *MW*.

A sketch of the fuel assembly seen from the top is shown in **Figure 2**, while in **Table 4** the main geometrical and physical parameters for the ALFRED FA are reported (Mansani, 2013). Figure 3 reports a lateral view sketch of the ALFRED Fuel Assembly.
A flow blockage at the beginning of the active region was considered here as the most critical case, for the reasons discussed in section 1.

For the correct description of the involved physical phenomena, the choice of the correct computational domain and boundary conditions is crucial. A wrong or superficial choice would lead to inaccurate or non-physical results. Almost the entire FA was modelled, without any symmetry planes and including the clad and wrap thermal structures and the bypass flow.

A sketch of the computational domain seen from the top is shown in Figure 4. The computational domain reproduces azimuthally the entire fuel sub-assembly, and periodic or symmetry boundary conditions are not needed. The model includes: the lead inside the FA, the pin clad, the FA wrap and the lead bypass. Symmetry boundary conditions are applied on the external side of the lead bypass. A 3D view of the modeled computational domain is shown in Figure 5. In the axial streamwise direction, the model includes: the entry non-active region, the active region, the downstream non-active region and the FA plenum. This latter allows to study the mixing phenomena and the detectability of the blockage. The streamwise vertical length of the different portion of the domain are summarized in Table 5. For all cases presented here, the blockage is located at the beginning of the active region as shown in Figure 6.

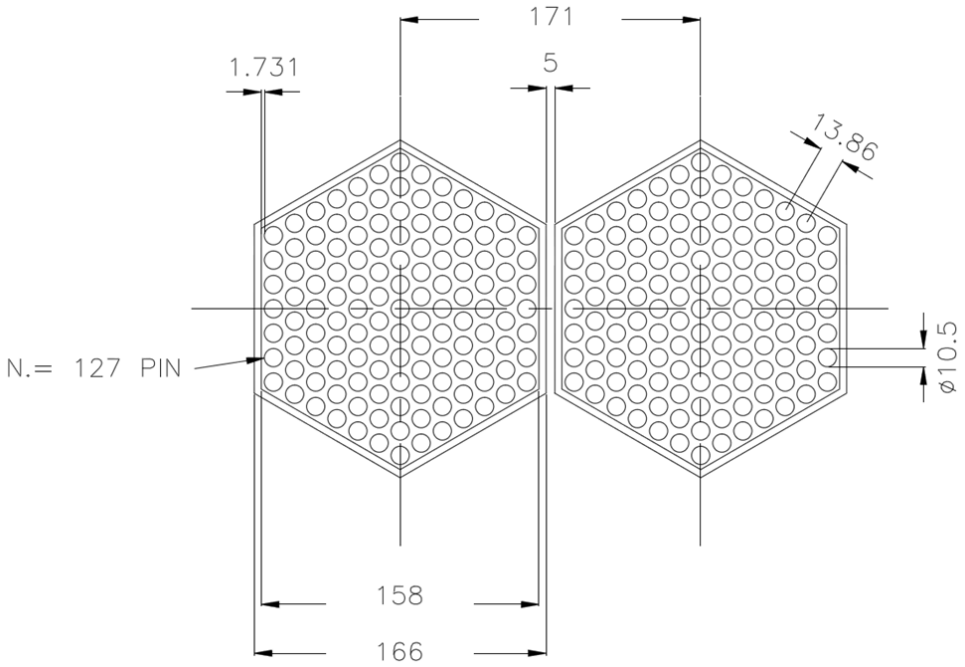

Figure 2 Sketch of the ALFRED Fuel Assembly: top view.

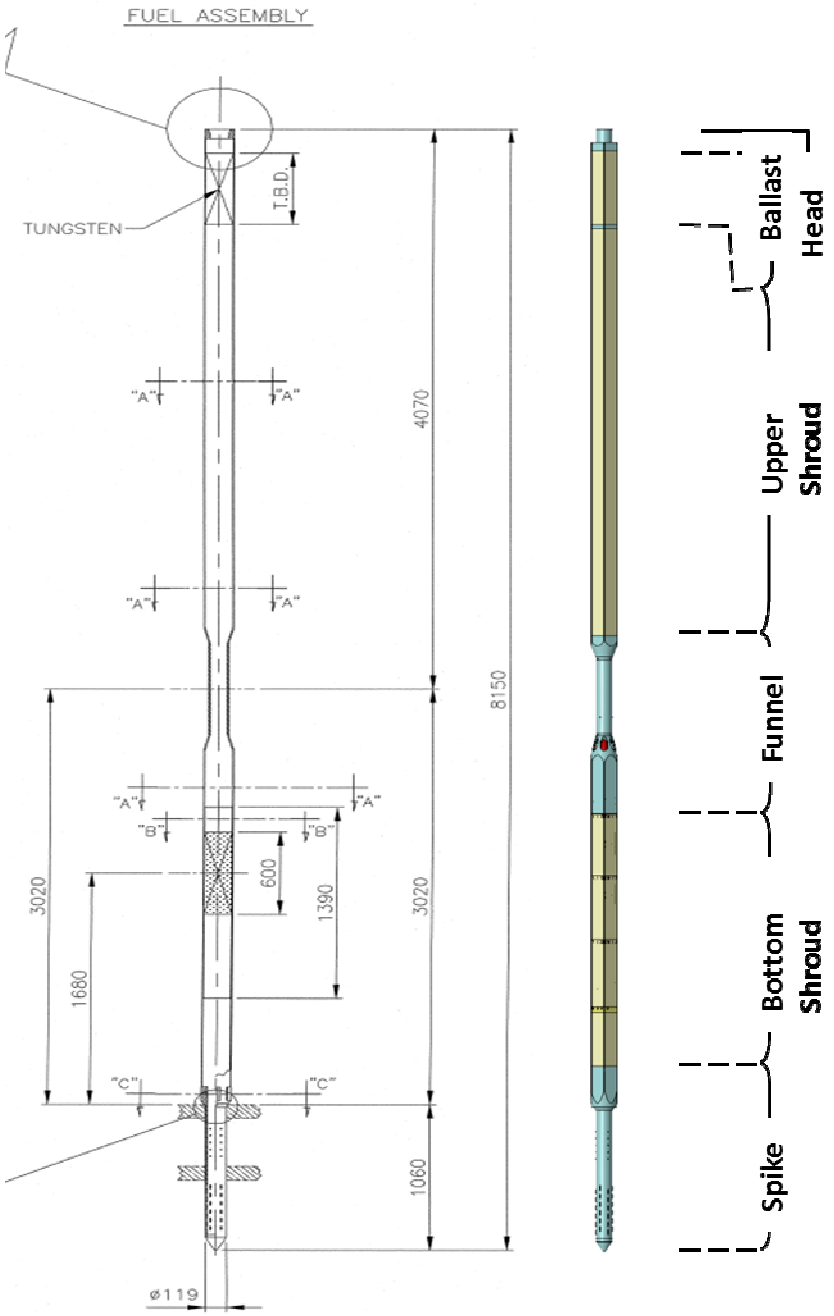

Figure 3 Sketch of the ALFRED Fuel Assembly: lateral view.

Table 4 Basic Geometrical and Thermal-hydraulic parameters of the DEMO ALFRED Core.

Rod diameter *d*	10.5 *mm*
Pitch to diameter ratio *p/d*	1.32
Subchannel Equivalent Diameter D_{eq}	9.68 *mm*
Number of fuel rods	127
Clearance between assemblies	5 *mm*
Assembly pitch	171 *mm*
Mean Assembly Power	1.75 *MW*
Mean Rod Power	13.814 *kW*
Mean Wall Heat Flux q_{wall}	0.7 MW/m^2
Conservative Wall Heat Flux (for engineering computations)	1 MW/m^2
Active Height *L*	0.6 *m*
Lead Inlet Temperature T_{inlet}	400 °*C*
Lead Outlet Temperature T_{outlet}	480 °*C*
Lead Bulk Velocity	1.4 *m/s*
Lead flow average FA	144.1 *kg/s*
Bypass flow average FA (3%)	2.76 *kg/s*
Clad Maximum Temperature (expected under nominal conditions)	550 °*C*
Total number of FA in the CORE	171
Total Reactor Thermal Power	300 *MW*

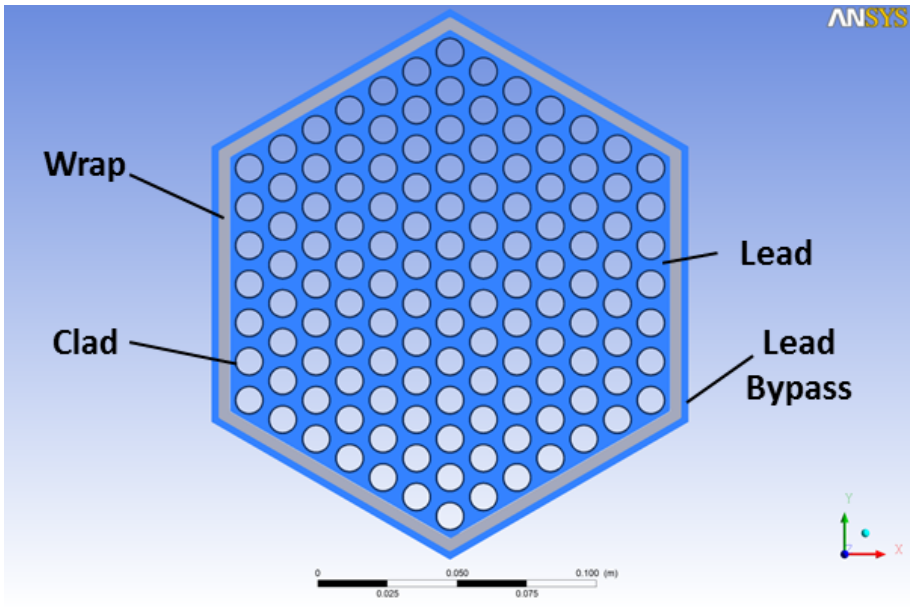

Figure 4 Computational domain for the CFD: top view.

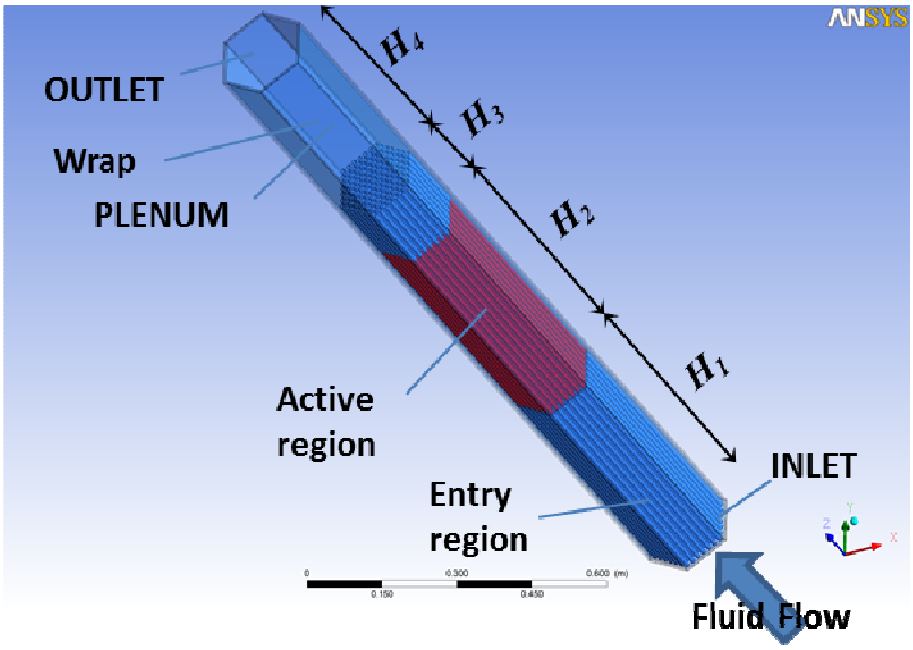

Figure 5 Computational domain for the CFD: perspective view.

Table 5 Main streamwise dimensions of the computational model of the ALFRED FA.

H_1	Entry	500 *mm*
H_2	Active	600 *mm*
H_3	Downstream	180 *mm*
H_4	Plenum	500 *mm*

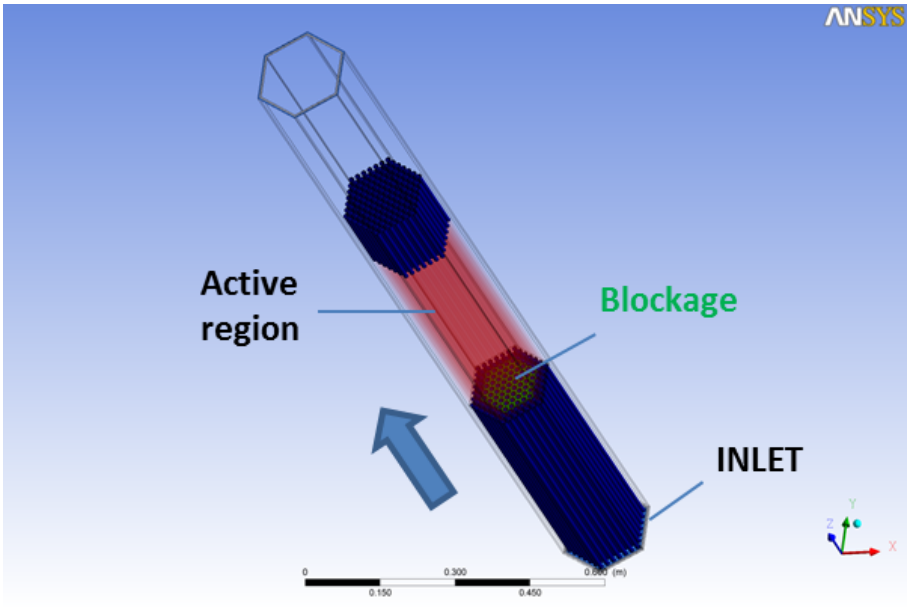

Figure 6 Computational domain for the CFD: blockage location.

For the unperturbed case without blockage, a total FA mass flow rate m=144.1 *kg/s*, constant temperature (T_{inlet}=400 °*C*), boundary conditions were imposed at the inlet coherently with the nominal data of Table 4 corresponding to the average FA, while pressure boundary conditions were imposed at the outlet. At the internal pin wall in the active region, a constant heat flux q_{wall}=1 MW/m^2 was imposed. This value represents a value corresponding to the highest power FA, and thus the analysis is conservative from an engineering point of view. The shape axial peaking factor in the active region has not been considered at this preliminary stage of the design of the FA.

Moreover, a bulk volumetric source term was evaluated from neutronic data and considered in the active part of the domain, to correctly keep into account the gamma power release. The imposed power density in the different portion of the domain are summarized in **Table 6.**

Table 6 Power density due to the gamma release in the FA.

Lead (FA)	10 MW/m^3
Wrap	15 MW/m^3
Lead (Bypass)	10 MW/m^3

For the cases with flow blockage, inlet mass flow rate boundary conditions were imposed coherently to preliminary RELAP5 computations for different area blockage fraction β (Bandini et al. (2013)). For an open element, a blockage does not induce any flow variation in the FA, i.e. the average velocity far upstream of the blockage remains unperturbed. On the opposite, for wrapped elements like the one under investigation here, a blockage increases the hydraulic resistance of the element itself, and the mass flow rate through the element is reduced according to the fraction of the area blocked. It has to be noted that the reduction of mass flow rate is not linear with the reduction of pass-through area, therefore the value of mass flow rate used for the simulation was provided by preliminary RELAP5 computations (Bandini et al. (2013)).

In **Table 7**, the computational test matrix is reported with the following fields: case number, simulation type (Stationary/Transient), Block Type (Central, Side, Corner), Number of blocked subchannels N_{block}, blocked area fraction β, inlet FA mass flow rate m, ratio between the mass flow rate m and the unperturbed value m_0=144.1 *kg/s*.

Table 7 Test matrix adopted for the flow blockage computations in the ALFRED FA

CASE Number	TYPE	BlockTYPE	N_{block}	β	m [*kg/s*]	m/m_0
0	STATIONARY	-	0	0.000	144.14	1.00
0TRANS	TRANSIENT	-	0	0.000	144.14	1.00
1	STATIONARY	CENTRAL	1	0.008	144.14	1.00
2	STATIONARY	CENTRAL	7	0.055	144.14	1.00
11	STATIONARY	CENTRAL	19	0.150	136.93	0.95
12	STATIONARY	CENTRAL	37	0.291	129.72	0.9

13	STATIONARY	CENTRAL	61	0.480	108.10	0.75
19	TRANSIENT	SIDE	3	0.024	144.14	1
20	STATIONARY	CORNER	3	0.024	144.14	1
21	STATIONARY	CENTRAL	19	0.150	136.93	0.95
28	TRANSIENT	CENTRAL	1	0.008	144.14	1
29	TRANSIENT	CENTRAL	7	0.055	144.14	1
30	TRANSIENT	CENTRAL	19	0.150	136.93	0.95

The computational mesh is multi-blocks fully structured with a resolution close to the wall such to achieve a y^+ of the order of 1 for the nominal FA mass flow rate. These features guarantee high accuracy to the model and minimize the discretization error and allow to integrate turbulence model equations down to the viscous sublayer. The total number of nodes is around $21.5 \cdot 10^6$, with 160 nodes in the axial direction. A mesh independence study was carried out, but it is not reported here, confirming that the used mesh provides results that are largely mesh independent.

Figure 7 reports the inlet view of the adopted computational mesh, with two levels of zoom on a pin and a subchannel, where the mesh resolution at the wall can be fully appreciated. Figure 8 reports the computational mesh at the outlet section, while Figure 9 is a perspective view of the active region with a zoom of the mesh in the blocked region. The vertical mesh resolution downstream the blockage is less than 2 mm.

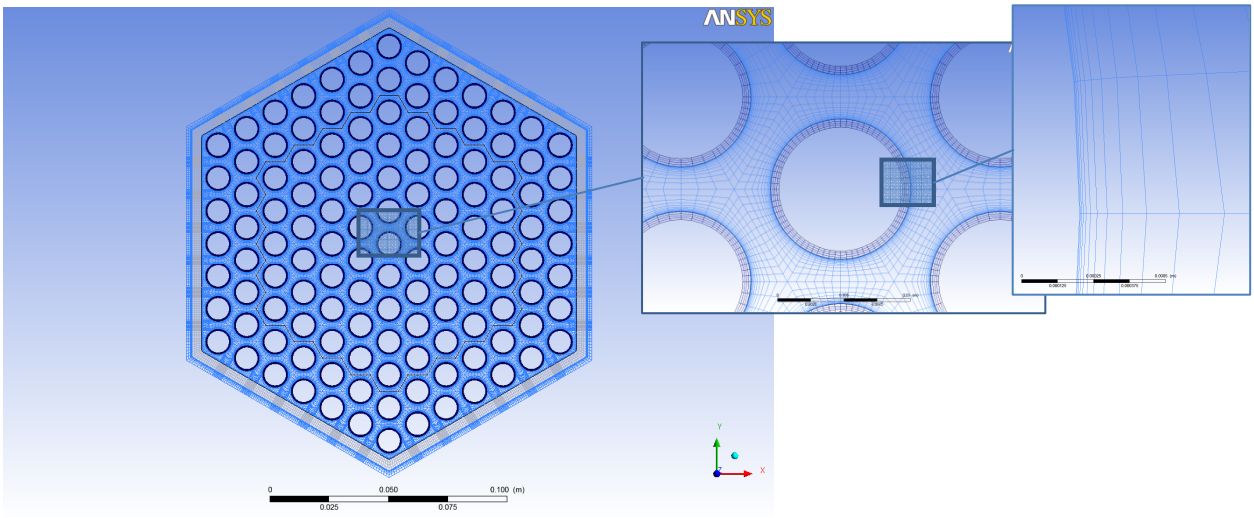

Figure 7 Computational mesh adopted: FA inlet. Two levels of zoom allows to appreciate the mesh resolution at the wall.

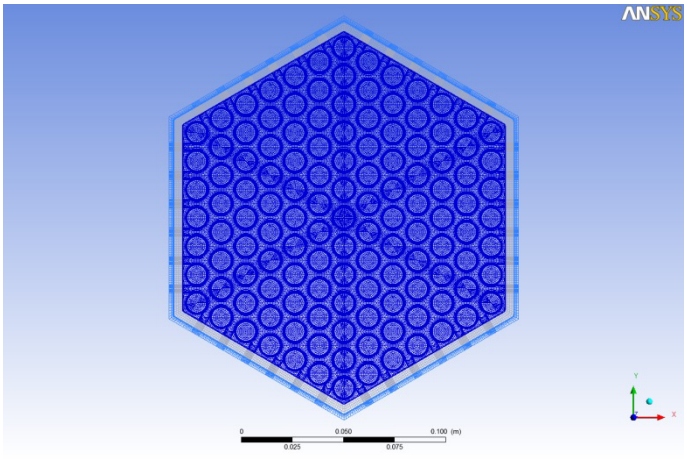

Figure 8 Computational mesh adopted: FA outlet.

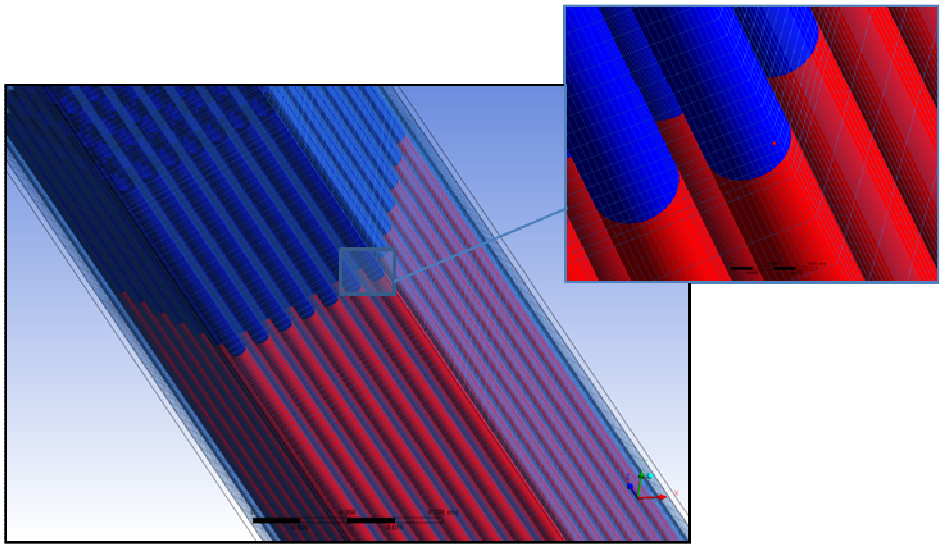

Figure 9 Computational mesh adopted: perspective view of the rods and zoom of the blocked area region. The vertical resolution downstream the blockage is less than 2 mm.

3.2. ALFRED FA RESULTS

3.2.1. Nominal unperturbed solution

The nominal unperturbed solution without any blockage is analyzed as a reference to check if the model provides reasonable results and to have the baseline to evaluate the effect of the blockage. The case was conventionally named case 0.

Figure 10 shows the *w* vertical velocity contours in a longitudinal transversal plane ZX of the computational domain. It is remarkable that the flow becomes hydro-dynamically fully developed before the beginning of the active region, and it confirms that the mechanical entry length is less than 10 hydraulic diameters. The other remarkable feature is the mixing phenomena at the beginning of the plenum region, see the zoom view in Figure 11.

Figure 12 shows the temperature contours in the fluid and in the thermal structures in the same longitudinal transversal plane ZX. The overall vertical temperature gradient is clearly visible and the outlet bulk temperature is about 503 °C as it is expected from a simple thermal balance based on the imposed heat flux and mass flow rate. Temperatures up to 530°C were reached at the end of the active region in the clad. Figure 13 shows a zoom view of the temperature contours in the same ZX plane with the superimposed velocity vector.

Figure 14 shows the vertical velocity contours in the XY plane in the middle of the active region, where the small hydrodynamic boundary layers close to the pins can be observed. In the proximity of the wrap, the contour shape is deformed due to the no-slip effect of the wall, both in the side and in the corner regions, with bulk values of 0.8-1 *m/s* in the side subchannels compared to 1.5-1.6 *m/s* in the internal ones.

Figure 15 shows the temperature contours in the XY plane in the middle of the active region. The central channel-wall temperature difference is of the order of ~50°*C*, while the bulk-wall temperature difference is ~40 °C with heat transfer coefficients based on this difference HTC~$2.4 \cdot 10^4$ W/m^2K and Nusselt numbers Nu~14. These data are coherent with the Nusselt numbers expected in liquid metals for the present Peclet number Pe~1200.

In **Figure 15**, a residual thermal coupling between subchannels with a non-uniform azimuthal wall temperature distribution can be clearly observed. The most relevant effect is the presence of the typical cold fluid regions in the subchannels close to the FA wall. This is an effect of the almost adiabatic conditions at the wall which imply a smaller power per unity mass flow rate in these subchannels with respect to the standard central subchannels. Another relevant feature is the presence of clad hot regions in the corner due to the lower heat transfer coefficient in the corner. This leads to an azimuthal temperature difference of ~50 °C in the clad of the corner pins with associated deformation and stresses. All these results are coherent to the authors' experience on the ICE Fuel Pin Bundle Simulator of the CIRCE facility (Di Piazza et al.(2013))

The computed pressure drop across the modeled FA is Δp_{IO}~25000 *Pa*.

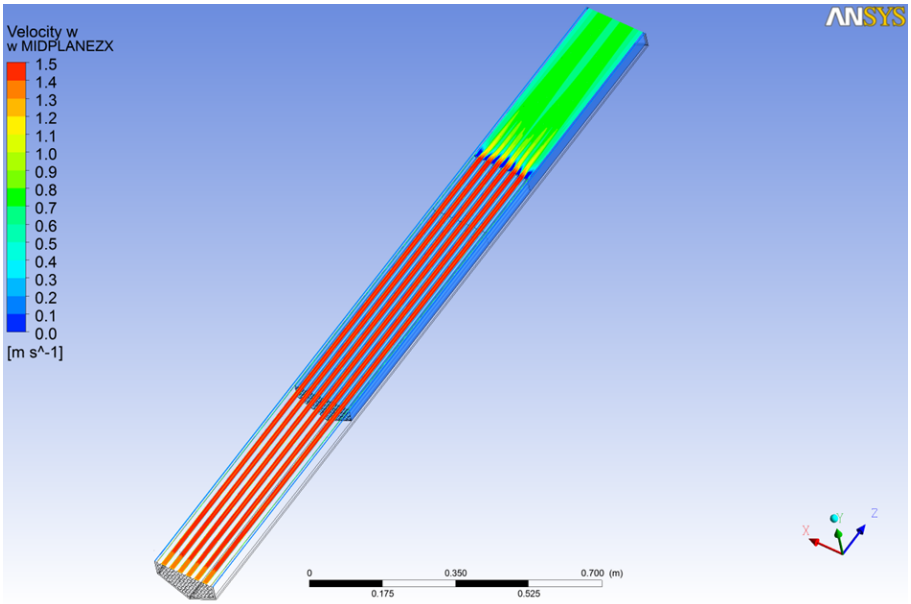

Figure 10 Streamwise velocity contours in the symmetry ZX plane.

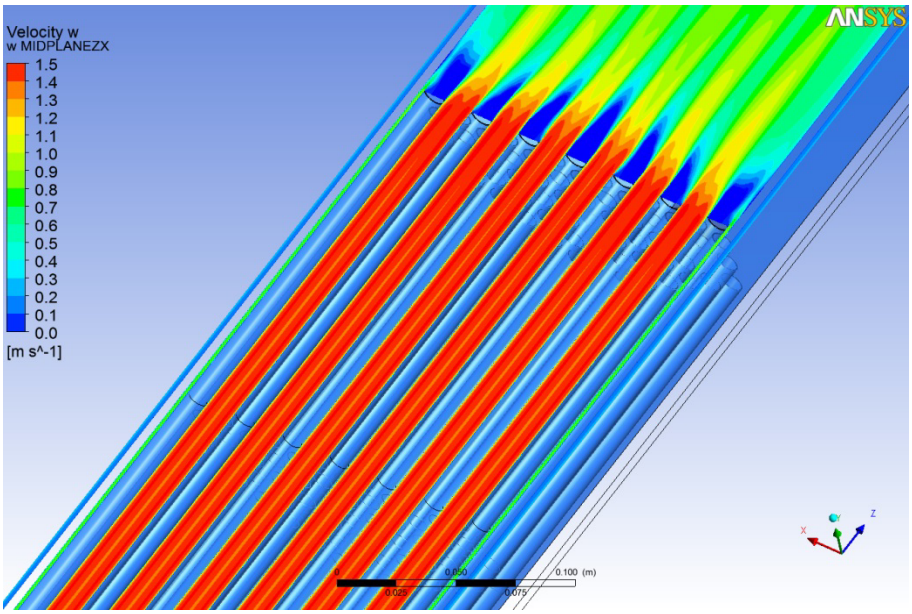

Figure 11 Streamwise velocity contours in the symmetry ZX plane: zoom view.

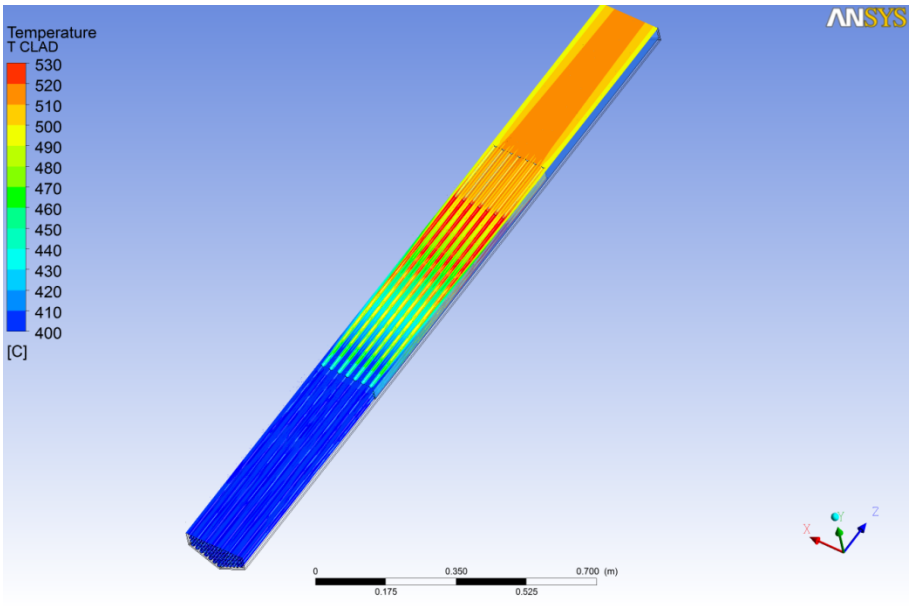

Figure 12 Temperature contours in the symmetry ZX plane.

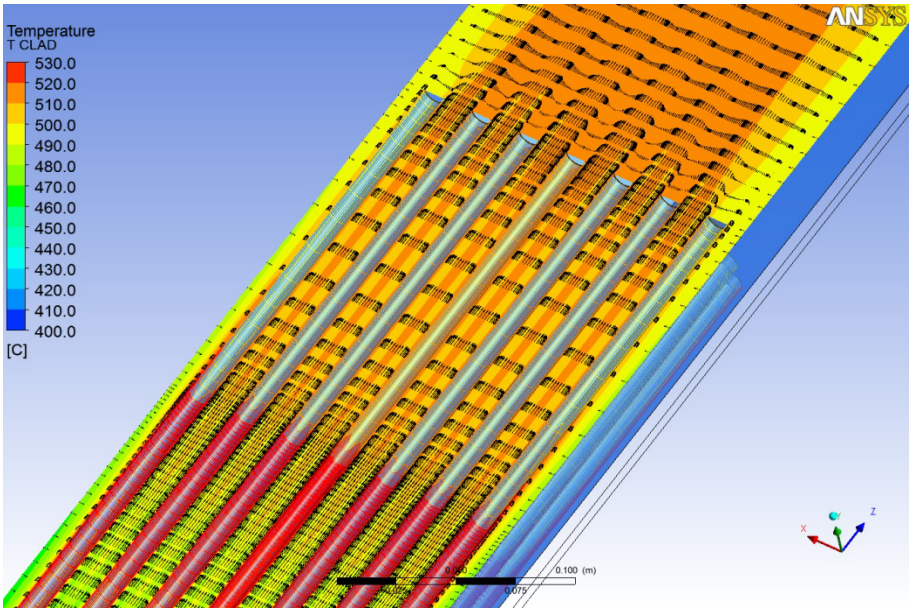

Figure 13 Temperature contours in the symmetry ZX plane with superimposed velocity vectors: zoom view

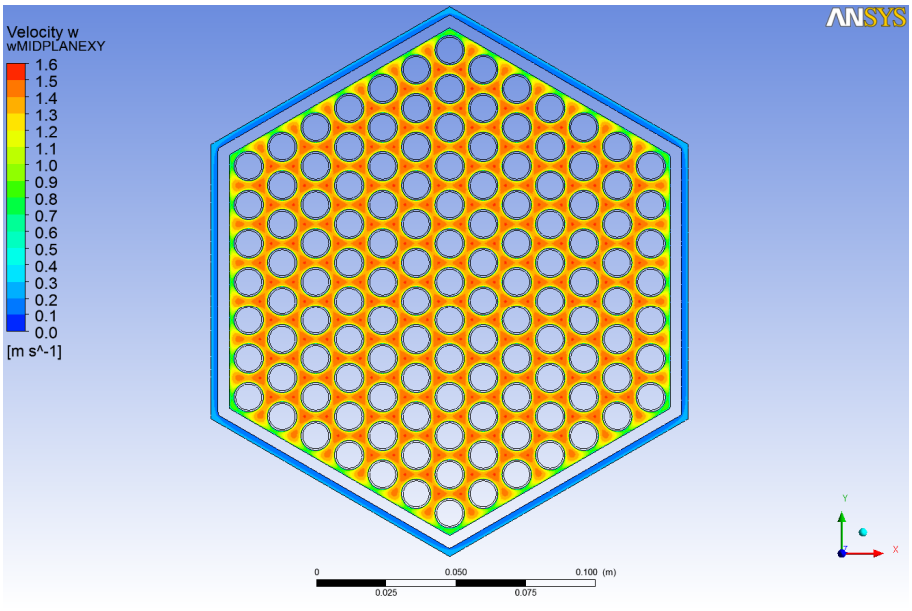

Figure 14 Streamwise velocity contours in the XY plane in the middle of the active region.

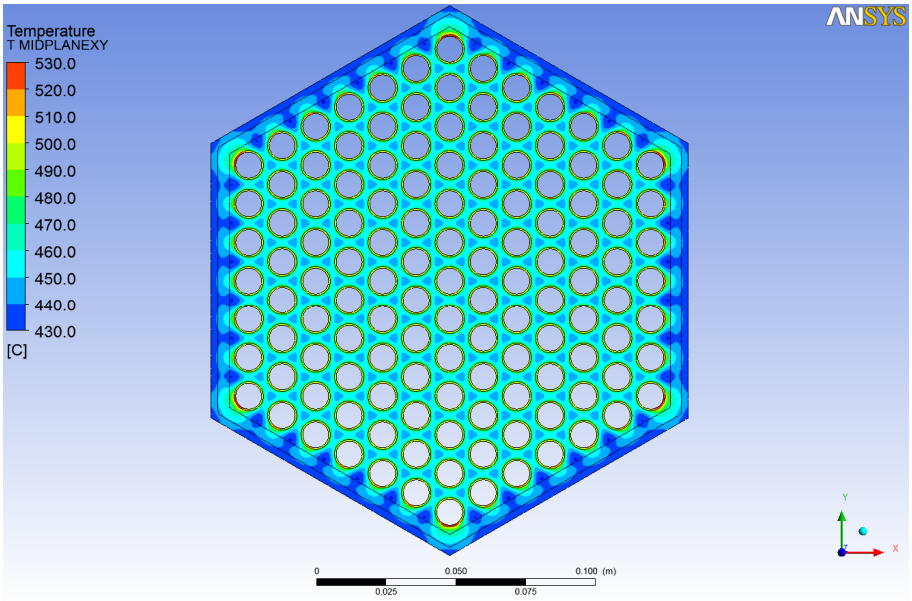

Figure 15 Temperature contours in the XY plane in the middle of the active region.

3.2.2. Comparison between CFD and system codes for foot blockage

The topic covered into the paper is the internal blockage of ALFRED lead-cooled FA. This is not easy to simulate with a system code due to the local phenomena involved. Due to the high boiling temperature of the coolant (1750 °C), different from sodium and water, the boiling of lead due to the blockage is virtually impossible, because before boiling the structural material would collapse. This fact implies that the flow is strictly single-phase and CFD methods are well tested in that case.

A comparison between CFD and SYS-TH methods is possible for foot blockage, where several system code analyses were carried out during the last FP7 projects and in papers.

RELAP5 simulations were presented by Bandini et al. (2013) on different accidental scenarios of the ALFRED reactor. In the paper, foot blockage with blocked area fraction β from 0.1 to 0.95 are simulated. Detailed data on the mass flow rate in the FA and the axial power distribution used in the RELAP computations were provided to the authors of the present paper (Bandini(2014)). The axial power density distribution per unit length q'[kW/m] adopted in the RELAP simulations is reported in **Figure 16**, where z_{active} represents the vertical coordinate from the beginning of the active region. In the RELAP model, the FA is considered adiabatic with respect to the neighbouring Fuel Assemblies, and therefore heat losses for lateral conduction were neglected.

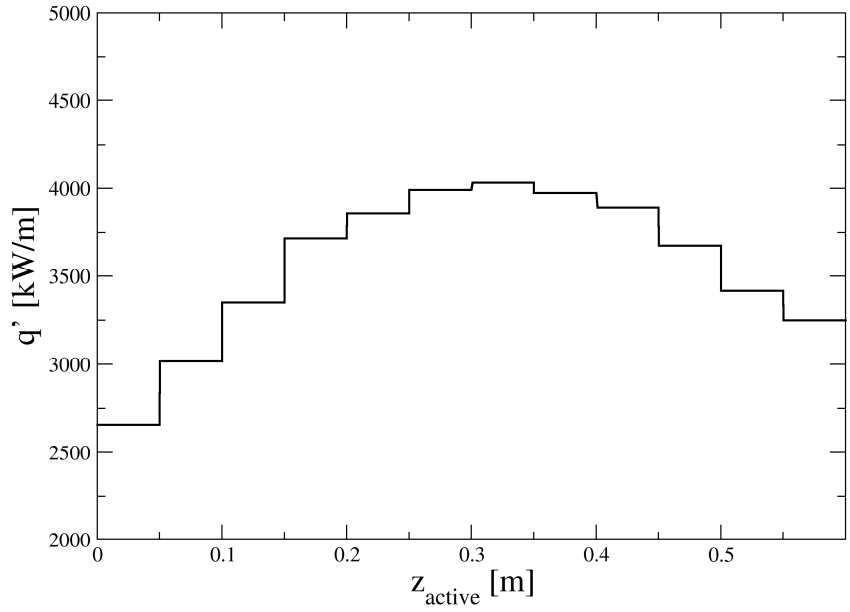

Figure 16 Power density distribution adopted in the RELAP5 computations.

Two test cases were simulated with CFD for comparison, for values of blocked area fraction β 0.8 and 0.9. The computational test matrix is reported in **Table 8**. Boundary conditions of the CFD model were fixed as coherent as possible with the RELAP model. Therefore the exact power density distribution in **Figure 16** was adopted in the CFD model and the FA was considered adiabatic by removing the wrap and the bypass from the CFD model. The computational mesh used for these calculations is the same adopted for the unperturbed solution in section 3.2.1, fully described section 3.1.

Table 8 Test cases adopted for the comparison between CFD and system code.

CASE Number	TYPE	BlockTYPE	β	*m* [*kg/s*]
CFR80	STATIONARY	FOOT	0.8	69.788
CFR90	STATIONARY	FOOT	0.9	37.066

Figure 17 and **Figure 18** reports the comparison between CFD and RELAP for CFR80 and CFR90 respectively. The comparison is in terms of bulk and clad axial temperature distributions in the active region. In both cases, the agreement is very good on the bulk temperatures in the whole active region. Regarding the clad temperature, the agreement is very good in the upper part of the active region with differences of 1-3 °C. Notably, CFD and RELAP5 predict the same maximum clad temperatures in both cases, i.e. ~635 °C and ~825 °C for β=0.8 and 0.9 respectively. The reason for the partial disagreement between the two codes in the lower part of the active region for T_{clad} is tied to developing of the thermal boundary layer which is captured by CFD: in the first 0.3 m the clad temperature profile is not parallel to the bulk temperature profile and the temperature difference between wall and bulk is not constant.

Considering these results, it can be definitely stated that the agreement between CFD and system code is very good for the foot blockage of the ALFRED FA.

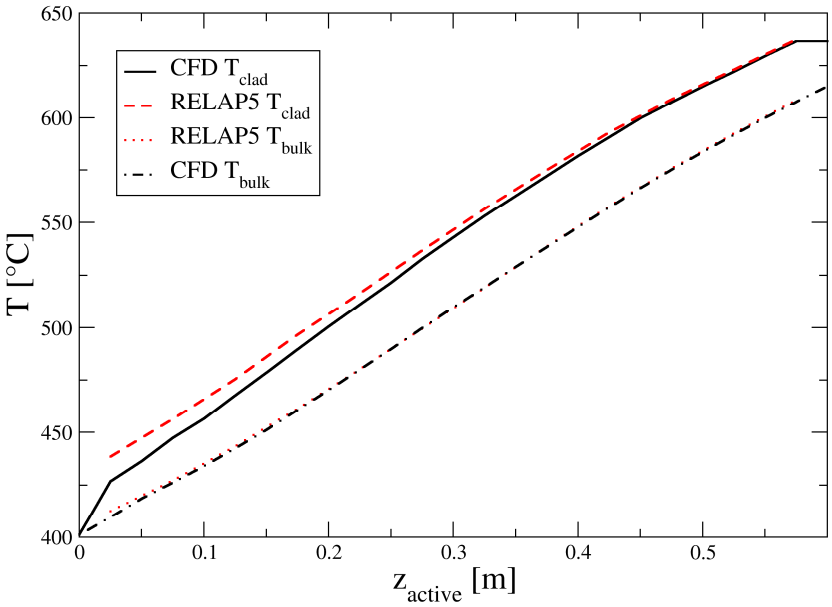

Figure 17 Comparison between CFD and system code (RELAP5) computations for 80% area foot blockage; z active is the vertical coordinate starting from the beginning of the active region. The bulk temperatures T_{bulk} and the clad temperature T_{clad} are reported.

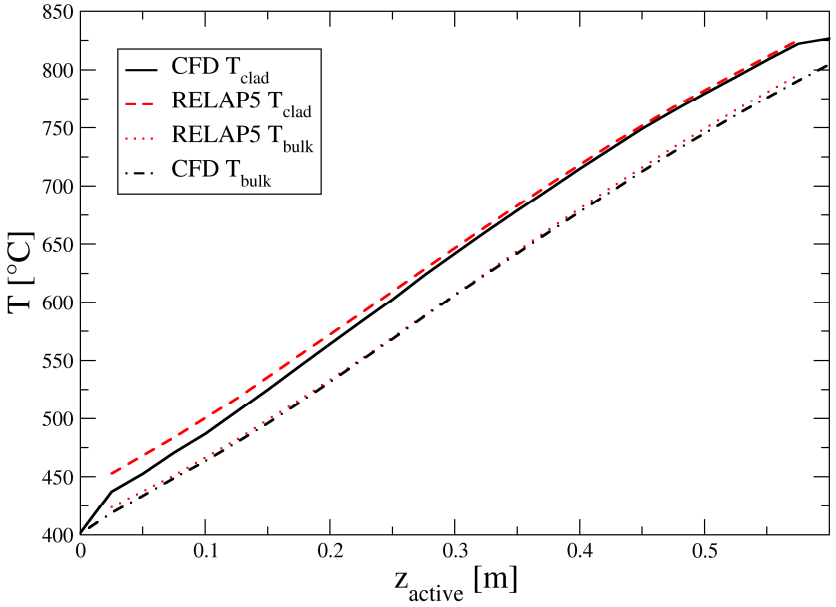

Figure 18 Comparison between CFD and system code (RELAP5) computations for 90% area foot blockage; z active is the vertical coordinate starting from the beginning of the active region. The bulk temperatures T_{bulk} and the clad temperature T_{clad} are reported.

3.2.3. Central blockage: stationary solutions (C1, C2, C11, C12, C13)

Several stationary solutions were computed with different degrees of central blockage. The neutronic feedback is not considered here.

For case 1 of Table 7 (one blocked subchannel), **Figure 19** shows the streamwise velocity distribution in the ZX midplane. From an hydrodynamic point of view, the perturbation on the flow caused by the blockage is local with a small recirculation region downstream the blockage and a slightly reduced

mass flow rate in the blocked subchannel. **Figure 20** shows the temperature field in the same ZX mid-plane. The dominant effect is an integral effect due to the reduced mass flow rate in the blocked subchannel. This leads to a *hot* subchannel with the associated mixing phenomena in the plenum region, and the maximum clad temperature at the end of the active region in the blocked subchannel.

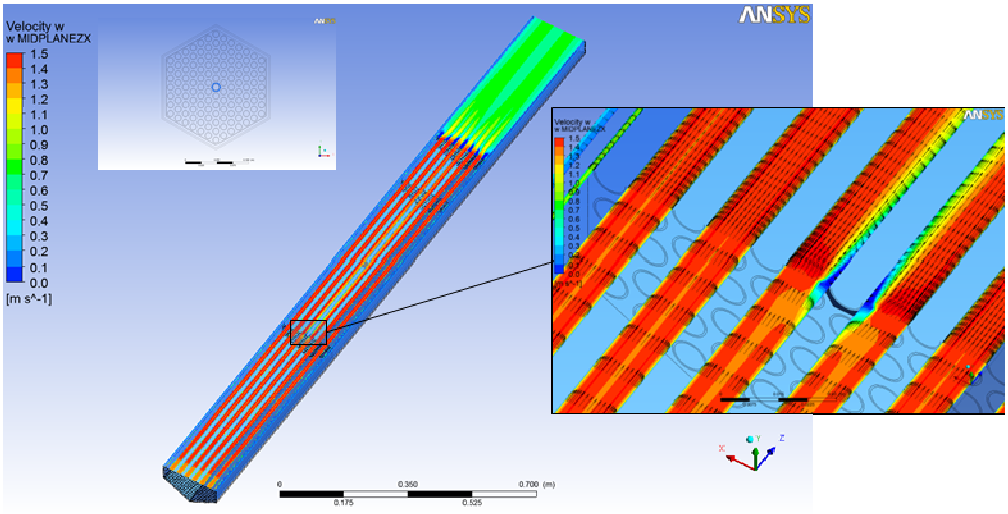

Figure 19 Streamwise velocity contours in the ZX midplane for case 1.

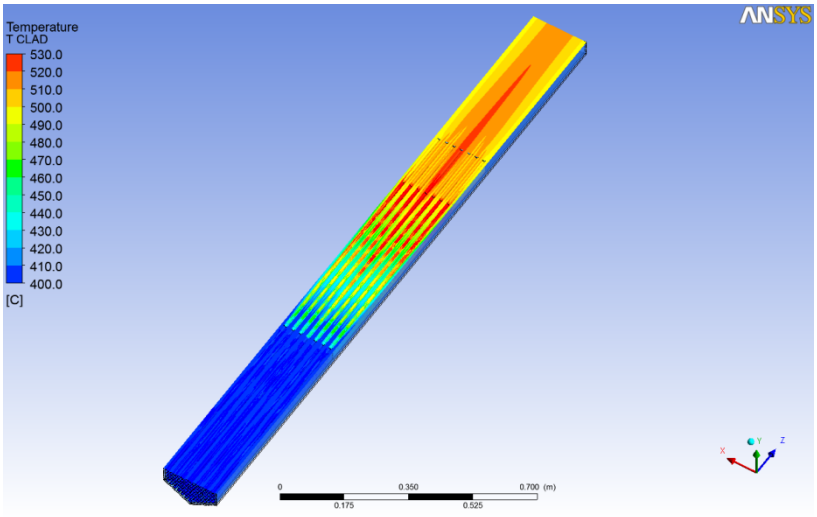

Figure 20 Temperature contours in the ZX midplane for case 1.

Figure 21 shows the streamwise velocity distribution in the ZX midplane for case 2 of Table 7 (seven blocked subchannels). From an hydrodynamic point of view, there is wake/recirculation region downstream the blockage and a reduced mass flow rate in the blocked subchannels. **Figure 22** shows the temperature field in the same ZX midplane. The dominant effect is the integral effect due to the reduced mass flow rate in the blocked subchannels. This leads to *hot* subchannels with the associated mixing phenomena in the plenum region, and the maximum clad temperature at the end of the active region in the blocked subchannels.

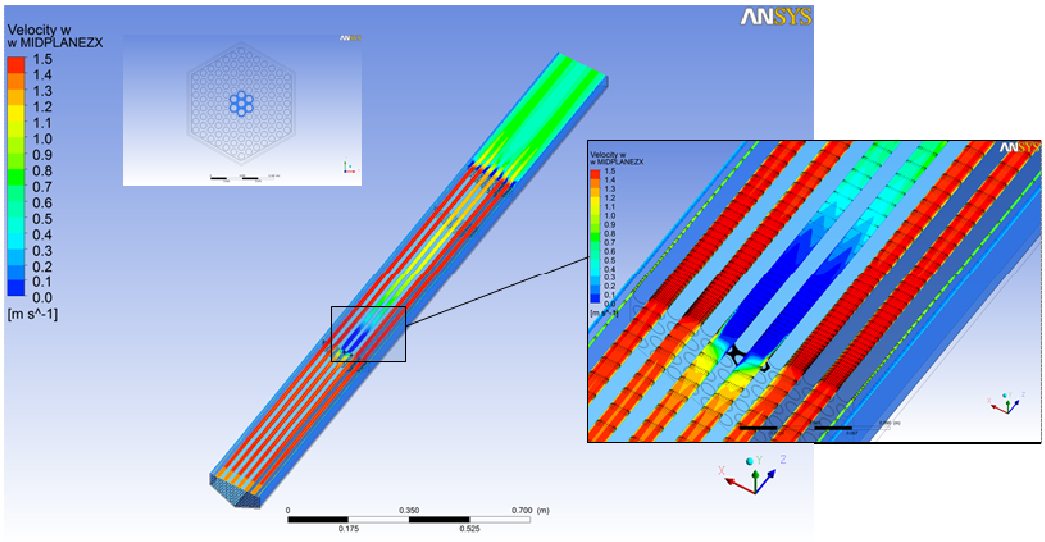

Figure 21 Streamwise velocity contours in the ZX midplane for case 2.

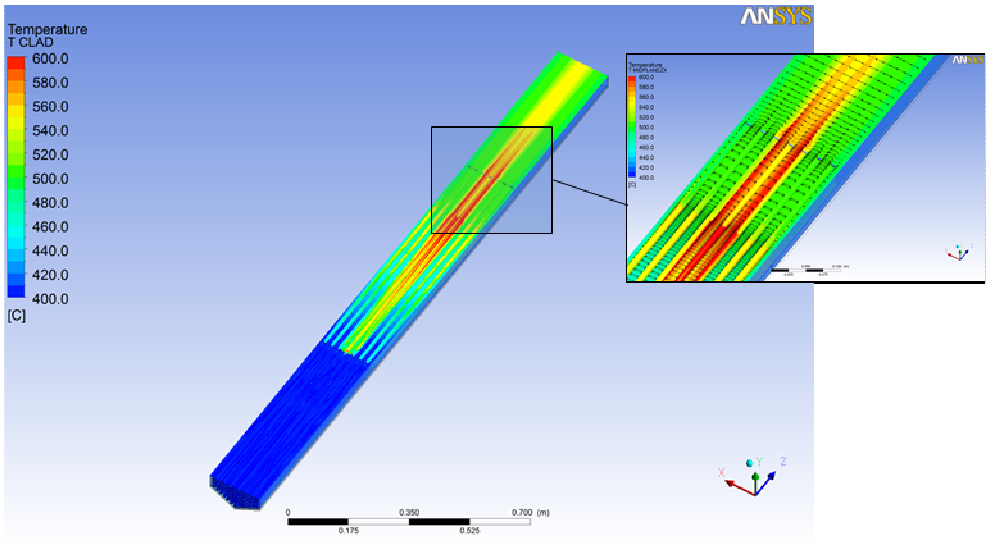

Figure 22 Temperature contours in the ZX midplane for case 2.

For case 11, the number of blocked subchannels is nineteen, i.e. three ranks, and the blocked area fraction β~0.15. **Figure 23** shows the streamwise velocity contours in the ZX midplane. A large recirculation region develops downstream of the blockage. The toroidal vortex is shear-induced by the flow in the non-blocked peripheral subchannels, see zoom view in **Figure 23**. The recirculating vortex downstream the blockage is elongated with an aspect ratio ~2-2.5. The central descending velocity is of the order of 0.8-1 *m/s* and guarantees good cooling conditions in the central pins of the blocked area downstream of the blockage. This fact is evidenced in **Figure 24**, where the temperature contours in the same XZ midplane are represented for case 11.

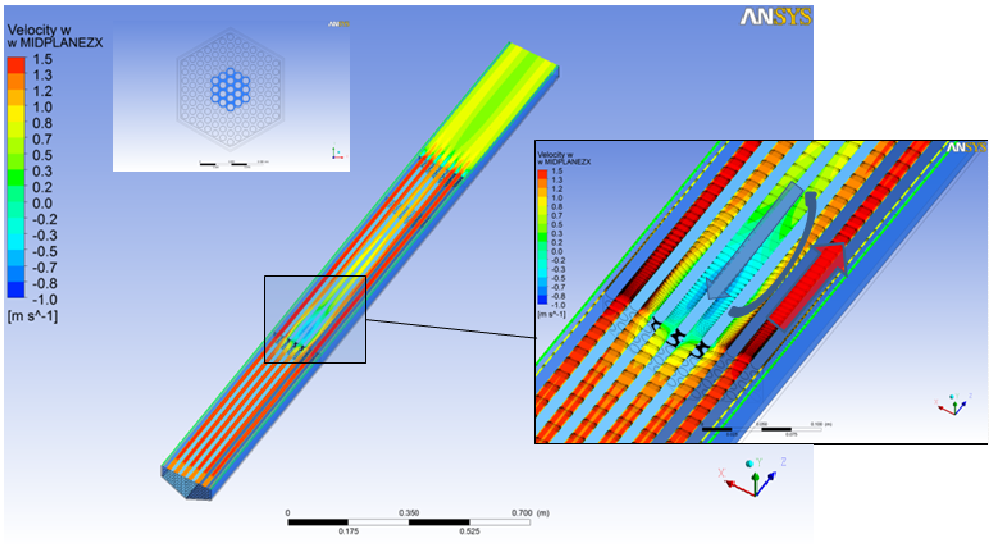

Figure 23 Streamwise velocity contours in the ZX midplane for case 11.

The maximum clad temperature downstream the blockage is not located in the central pins of the blocked region, but at the center of the toroidal recirculating vortex; therefore in the ZX midplane two maxima can be evidenced. Another temperature maximum is located at the end of the active region in the central pin. This maximum is due to the lower mass flow rate in the blocked subchannel and it can be view as an integral effect. In case 11, the clad temperature maxima downstream the blockage and at the end of the active region are of the same order, i.e. ~740 °C.

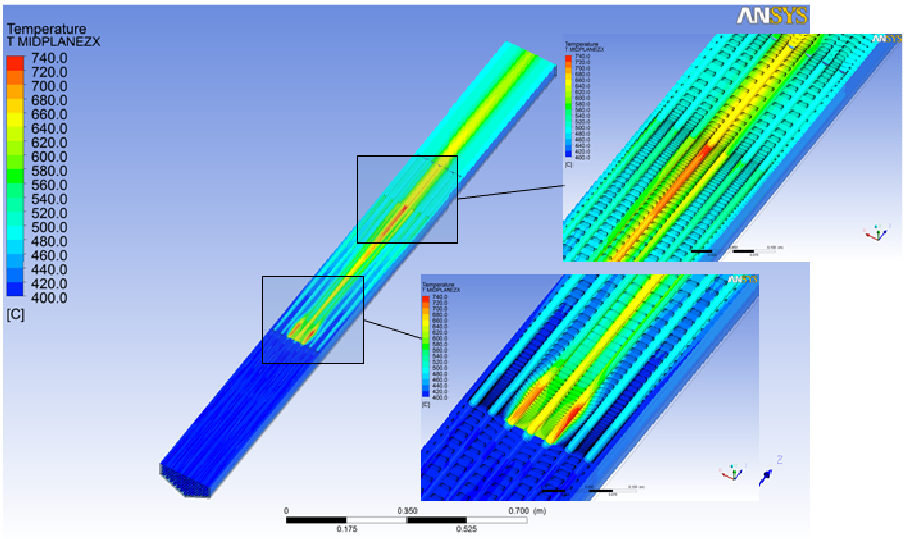

Figure 24 Temperature contours in the ZX midplane for case 11.

For case 12, with thirty-seven blocked subchannels (4 ranks), blocked area fraction β~0.29, qualitatively similar phenomena can be evidenced,. Figure 25 and Figure 26 show the streamwise velocity and temperature contours for the ZX midplane. For this larger blockage, from the heat transfer point of view, the dominant phenomena becomes the recirculating vortex downstream of the blockage, where temperatures around 1000 °C, are reached in the coolant.

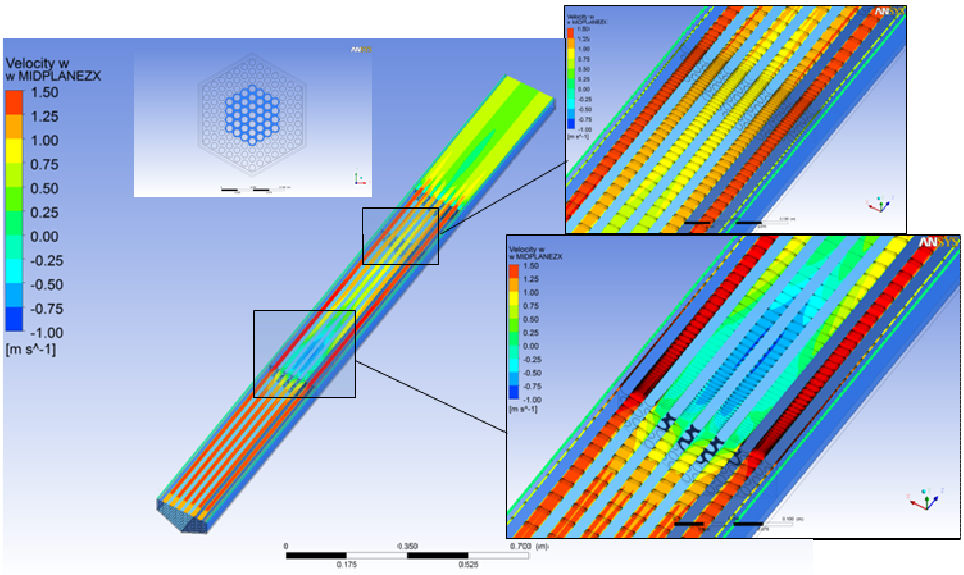

Figure 25 Streamwise velocity contours in the ZX midplane for case 12.

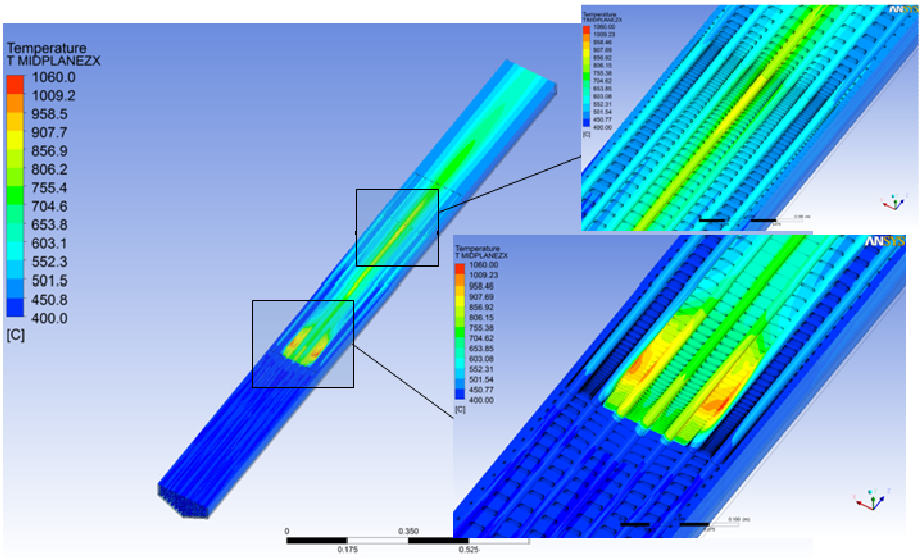

Figure 26 Temperature contours in the ZX midplane for case 12.

Figure 27 and **Figure 28** show the streamwise velocity and temperature contours for the ZX midplane for case 13, 37 subchannels (5 ranks) blocked, blocked area factor β~0.48. In this case almost 50% of the flow passage area is blocked, and a large recirculation shear-induced toroidal vortex develops downstream of the blockage section. The maximum clad temperature in the stagnation points in the vortex center is ~1500 °C.

As final remark, it can be noticed that on the maximum clad temperature the integral fluid dynamic effect due to the reduced mass flow rate in the blocked subchannel is dominant for small blockages (β<0.1), with the clad absolute maximum temperature located at the end of the active region in the central blocked pin. For large blockages (β>0.2), the dominant phenomena is the recirculation vortex and the clad absolute maximum temperature is located downstream the blockage in the center of the

vortex (stagnation point) in the peripheral pins of the blockage. In this case the maximum at the end of the active region is present but it is less important.

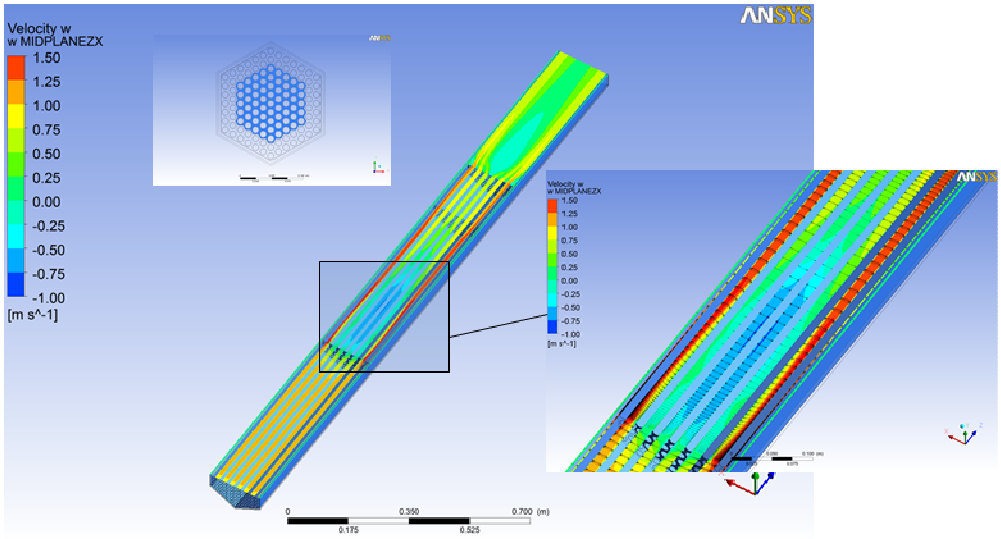

Figure 27 Streamwise velocity contours in the ZX midplane for case 13.

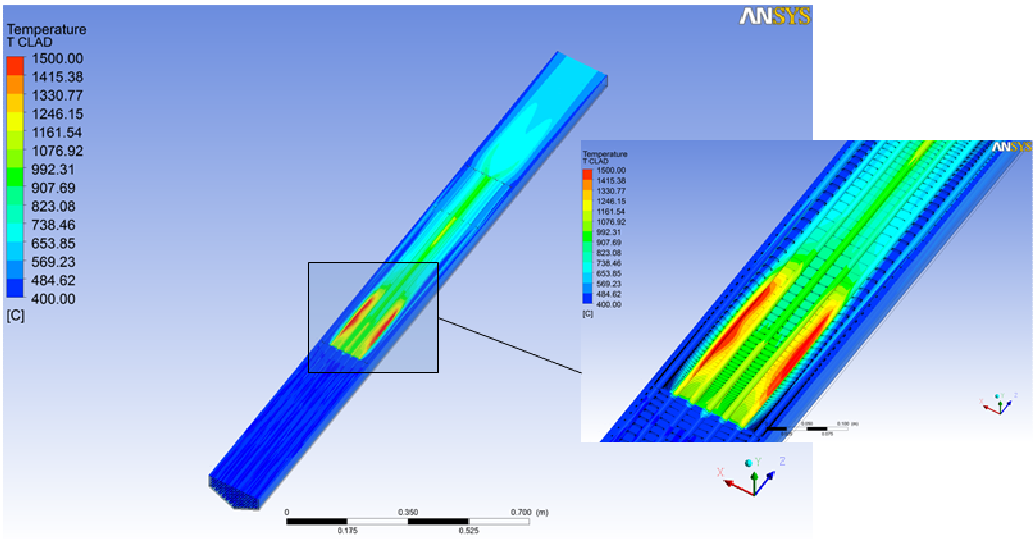

Figure 28 Temperature contours in the ZX midplane for case 13.

3.2.4. Central blockage: transient solutions (C28, C29, C30)

Starting from the stationary unperturbed solution case 0, some transient calculations (URANS) were carried out with the same computational features (mesh, boundary conditions, turbulence models) of the corresponding stationary cases. In particular, case 28, case 29, and case 30 of Table 7 refer to 1, 7

and 19 subchannels blocked respectively, and they must be compared with the corresponding stationary cases 1, 2 and 11.

The monitoring points in the following graphs are located in the central subchannel of the FA, at different vertical coordinate *z*: P1 in the middle of the active region, P2 at the outlet of the active region, P3 at the end of the rod, P4 at the outlet section of the FA. P5 is located at the outlet section of the FA 10 mm far from P4.

Figure 29 shows the streamwise time velocity behaviour in some monitoring points for case 28 (N_{block}=1). The time-dependent simulation actually starts at t~1.5 *s*, from unblocked Initial Condition case 0 see the blue line in the figures. **Figure 30** shows the temperature time dependent behaviour in the same monitoring points; P_{max} shows the maximum temperature in the clad. Some relevant considerations yield:

- ✓ The hydrodynamic and thermal time scales of the transient are similar and of the order of 1-1.5 *s* in this case (small blockage); the maximum clad temperature is ~580 °*C* and this confirms results from stationary simulation case 1.

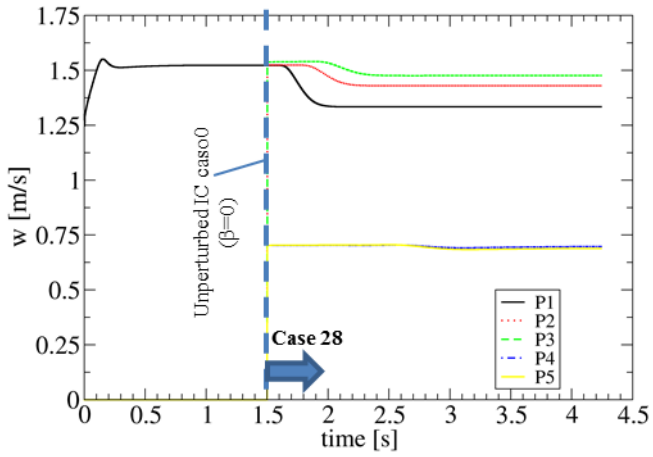

Figure 29 Streamwise velocity *w* against time in some monitoring points for case 28

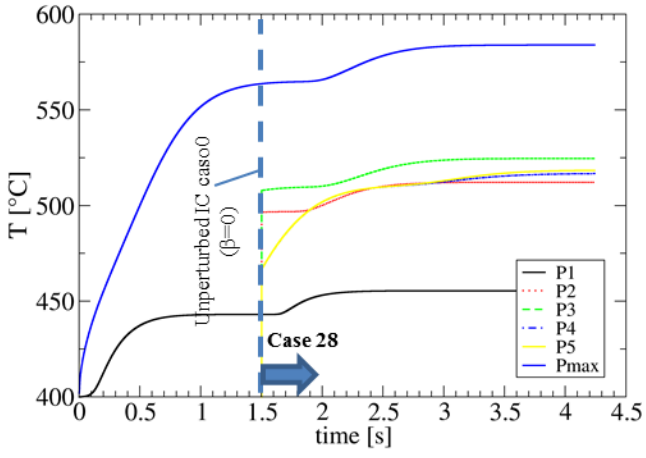

(N_{block}=1).

Figure 30 Temperature against time in some monitoring points for case 28 (N_{block}=1).

Figure 31 and **Figure 32** show the same quantities as **Figure 29** and **Figure 30** for case 29 (N_{block}=7). In this case the time-dependent simulation actually starts at t~2.8 *s* from unblocked Initial Condition case 0,

see the blue line in the figures. Hydrodynamic and thermal time scales are of the order of 1.5-2.0 *s*, and the maximum clad temperature is of the order of 650 °C.

Figure 33 and **Figure 34** show the same quantities for case 30 (N_{block}=19). In this case, the velocity field reaches its statistical asymptotic distribution in ~1.5 s, while the duration of the temperature transient is of the order of 3-4 *s*.

Figure 35 shows the temperature contours for the case 30, time=9 *s*. The distribution reflects the phenomenology described in the previous section for the large blockages, and the maximum clad temperature is ~800 °C, of the same order to the value obtained in the corresponding stationary case 11.

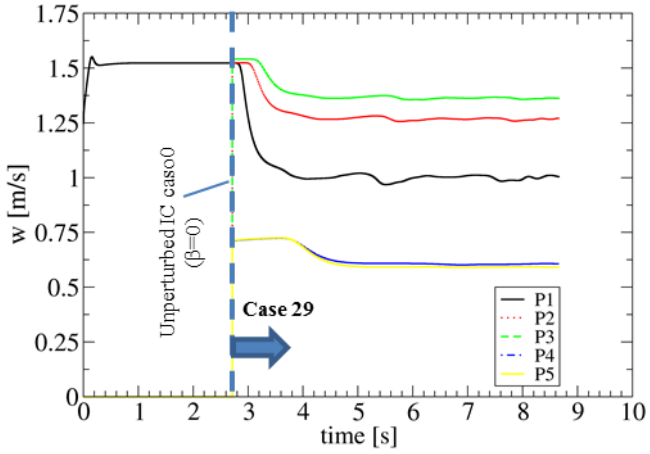

Figure 31 Streamwise velocity *w* against time in some monitoring points for case 29 (N_{block}=7).

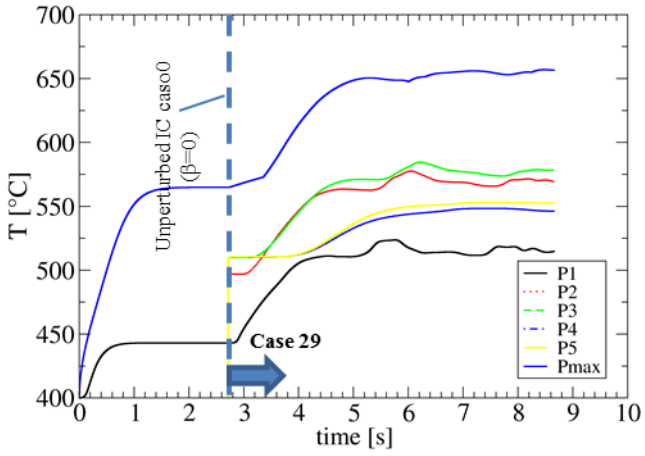

Figure 32 Temperature against time in some monitoring points for case 29 (N_{block}=7).

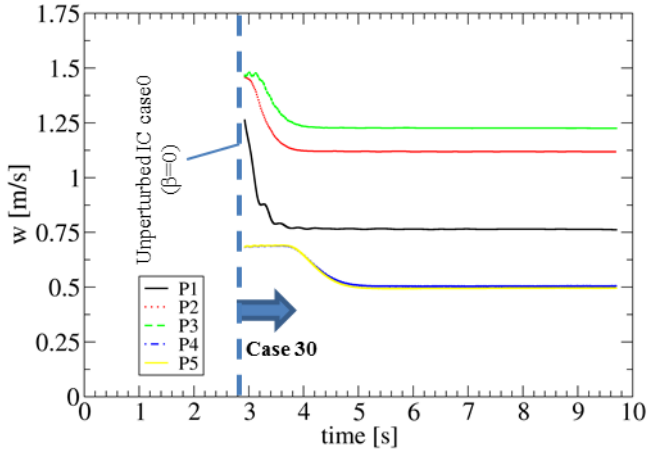

Figure 33 Streamwise velocity *w* against time in some monitoring points for case 30 (N_{block}=19).

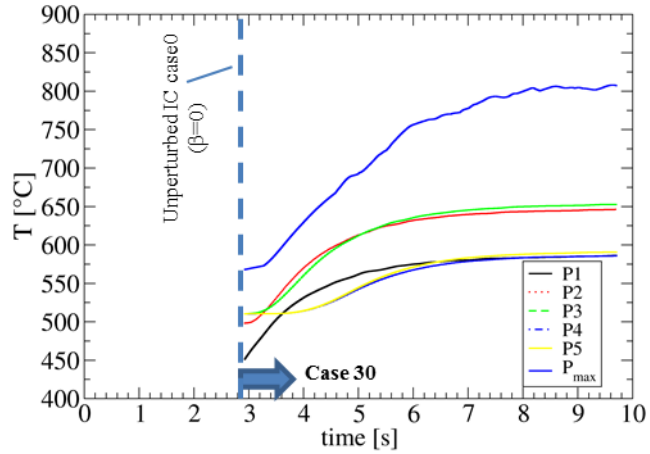

Figure 34 Temperature against time in some monitoring points for case 30 (N_{block}=19).

Figure 36 shows the temperature contours in the mixing region of the FA and in the outlet section for case 30 (N_{block}=19). Time t=2.8 s represents the starting initial time for the blockage from an unperturbed condition. The temperature scale was fixed according to the 'asymptotic' temperature distributions at the end of the transient with a temperature difference across the outlet section of ~100 °C. The first comment to this picture is that the mixing in the FA plenum region is not very effective and the temperature distribution at the outlet section is not uniform in the case of a blockage. The detectability of the blockage by temperature measurements at the outlet section is possible after 1 *s* from the abrupt event; in the present 'case 30'; after 2 s a maximum temperature difference in the section of ~50 °C can be evidenced.

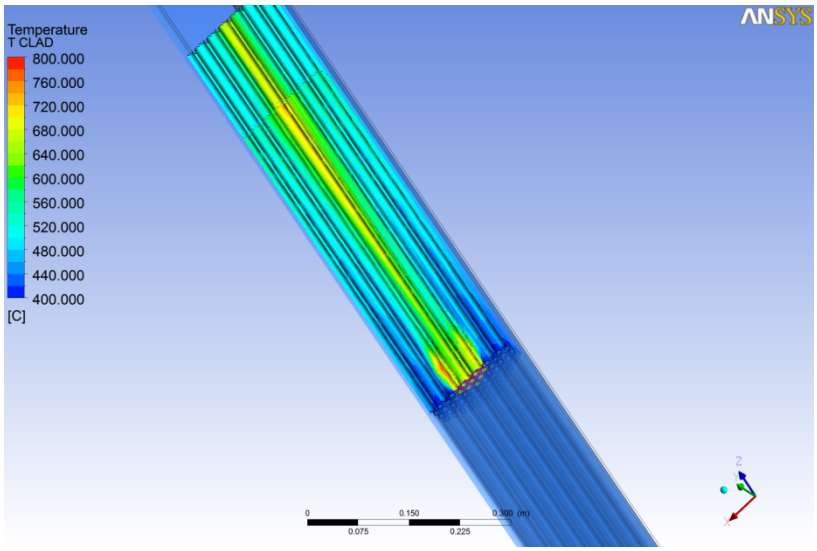

Figure 35 Clad temperature contours for case 30 (N_{block}=19): time = 9 *s*.

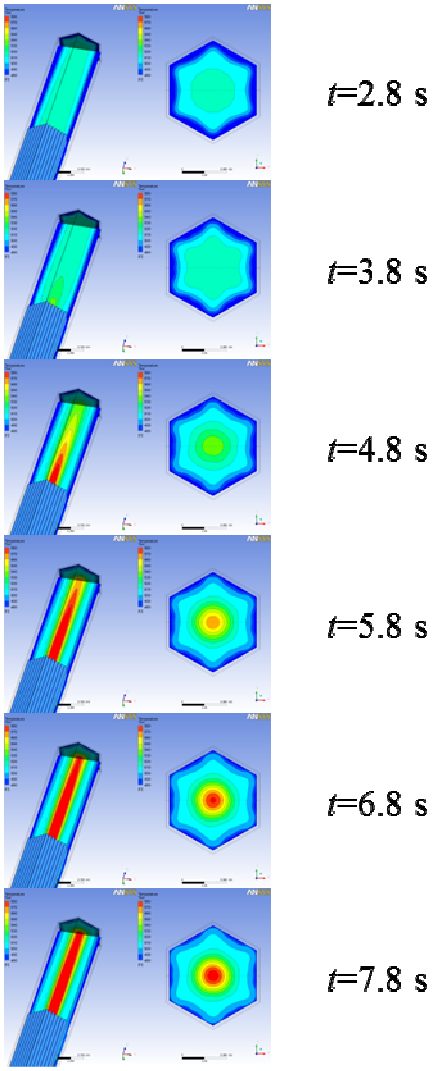

Figure 36 Temperature contours in the mixing region of the FA and in the outlet section for case 30.

3.2.5. Discussion on the relevant engineering parameters

From a safety point of view, the most important parameter to monitor and detect is the maximum clad temperature. **Table 9** shows the maximum clad temperatures in the recirculation region downstream the blockage ($T_{max,loc}$) and at the end of the active region ($T_{max,end}$) for the cases simulated with central blockage. **Figure 37** shows the 2D graph of the same quantities versus the blockage area friction factor β for all the simulated cases.

As it has already been stated, for small blockages (β<0.1) the absolute maximum clad temperature is located at the end of the active region, with the square symbols higher than the circle symbols. For the highest levels of blockage (β>0.2) the absolute maximum clad temperature is located in the recirculation region downstream the blockage, with the circle symbols higher than the square symbols. From **Table 9** and **Figure 37**, it can be evidenced that maximum clad temperatures larger than 1000 °C can be reached for blockage area fraction β>0.3 (37 subchannels). Moreover, as already stated in the previous section, stationary and transient cases lead to similar results in terms of maximum clad temperatures.

Regarding the detectability of the blockage, a simple method could adopt thermocouples in the plenum region of the FA. **Table 9** reports the maximum transversal temperature drop ΔT_{out} at the outlet section of the modelled FA for each case. This quantity depends on the degree of blockage and on the mixing phenomena in the plenum region of the FA. The mixing phenomena can be correctly predicted by CFD and therefore the value of ΔT_{out} can be considered realistic. It is interesting to notice that small blockages (cases 1, 2) are not easy to detect because the temperature drop does not differ very much from the unblocked case. Large blockages (cases 11, 12 ,13) with β >0.15 in principle could be detected because the temperature drop in the section reaches 100 °C or more.

It must be stressed that the maximum clad temperatures reported in this paper differs significantly from the blockage computations reported in analysis carried out by system codes (Bandini et al. (2013)). This is because the system codes analysis can only investigate the foot blockage and quantify the subsequent mass flow rate decrease; this decrease implies an increase of the average bulk inlet-outlet FA temperature drop and therefore an increase of the clad temperature at the end of the active region. Therefore the system code analysis only consider the 'global effect' and average the effect itself in all the subchannels. On the other hand, CFD analysis can quantify the 'global effect' in the blocked subchannels and it can fully described a new physical effect, i.e. the stagnation point in the wake recirculation region behind the blockage. It was shown that this latter phenomenon becomes dominant for relatively high degrees of blockage (β>0.1) and therefore the analysis by system codes of such kind of accident completely fails in these conditions.

Table 9 Maximum temperatures for several cases at different degree of blockage.; $T_{max,\ loc}$ and $T_{max,end}$ refer to the clad temperatures.

CASE Number	TYPE	BlockTYPE	N_{block}	β	m [kg/s]	m/m_0	$T_{max,loc}$ [°C]	$T_{max,end}$ [°C]	ΔT_{out} [°C]
0	STATIONARY	-	0	0.000	144.14	1.00	442	**530**	18
1	STATIONARY	CENTRAL	1	0.008	144.14	1.00	450	**580**	21
2	STATIONARY	CENTRAL	7	0.055	144.14	1.00	584	**605**	55
11	STATIONARY	CENTRAL	19	0.150	136.93	0.95	**734**	**722**	108
28	TRANSIENT	CENTRAL	1	0.008	144.14	1.00	450	**584**	25
29	TRANSIENT	CENTRAL	7	0.055	144.14	1.00	565	**657**	55
30	TRANSIENT	CENTRAL	19	0.150	136.93	0.95	**800**	722	90
12	STATIONARY	CENTRAL	37	0.291	129.72	0.9	**1030**	820	135
13	STATIONARY	CENTRAL	61	0.480	108.10	0.75	**1550**	1250	140

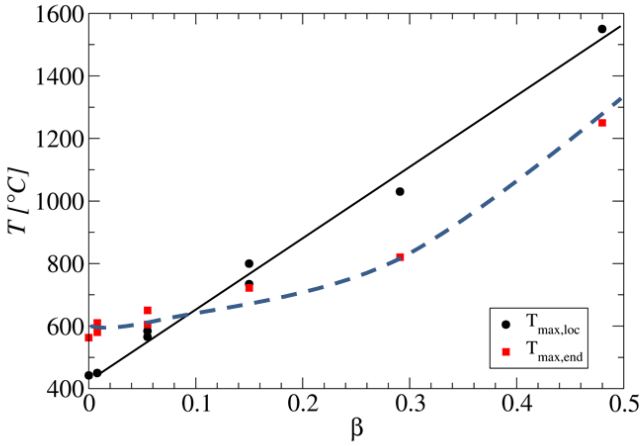

Figure 37 Maximum clad temperature versus the blockage area factor β from the CFD computations for central blockage located at the beginning of the active region: $T_{max,loc}$ is the temperature maximum behind the blockage, while $T_{max,end}$ is the maximum temperature at the end of the active region.

4. Neutronic feedback assessment

4.1 Coupling methodology and models

Flow blockage analysis in nuclear reactors involves a coolant mass flow partial or total reduction simulating debris accumulation and subsequent blockage. A drop in heat transfer coefficient is induced, causing fuel and cladding temperature to rise. Present study aims at providing more details with respect to previous evaluations – namely considering neutronic thermal feedback as far as central channel heating up is concerned.

The present section is devoted to a preliminary quantification of the neutronic feedback effect on the power and on the temperature field. The methodology is based on an evaluation of the feedback coefficients via the ERANOS 2.1 code. These coefficients are then used to quantify the reactivity insertion due to the thermal transient obtained by the CFD analysis in a stable reference point represented by the operating point (Normal Condition).

Power evolution within a nuclear reactor is related to neutron flux change as the local power generation term is proportional to flux through fission reaction macroscopic cross sections. Exact time-dependent model in a general 3D domain would be expected to solve neutron transport equation according to time - determining point-wise neutron population behaviour. Such a description is coupled to a thermal-hydraulic analyses following cross section variation depending on temperature variation. Nuclear data and cross sections are updated at every calculation step and transients are represented.

Flow blockage accident was preliminarily simulated and turned out to be a quite local phenomenon for which a detailed geometry is necessary to be modelled in order to obtain representative results. According to the literature, a complete simulation at this stage would not be capable of considering all blocked sub-channels since the whole neutronic system – namely the reactor core – would be considered in a somewhat time-consuming approach. In addition, design verification is carried out in parallel to design review and updating. Straightforward verification is then required to support safety checks for system reliability. Therefore, a simple and easy-to-manage method is needed to iterate and provide timely design feedback.

A one-way coupling is here presented between ERANOS neutronic code and ANSYS CFX fluid dynamic tool. In considering neutron kinetics for reactor studies, it is commonly a matter of matching:

- Spatial description and point-wise flux behaviour evaluation according to local effects;
- Integral system analysis through lumped parameters approach;

System lumped parameters are related to the multiplication factor and time coefficients as well as delayed neutron fraction and related decay constants. The latter approach is mainly followed since mathematical model is simple and calculation tools may treat it in a quite straightforward manner.

In order to take advantage of reactivity effect due to both local parameters variation and integral lumped analysis provided by point-wise kinetics, a two-step process is implemented and described hereafter.

Foremost, the ERANOS neutronic deterministic code is used and local system variations are applied to representative and effective parameters:

- Fuel temperature (Doppler effect) (assumed +350 °C in neutronic calculation);
- Fuel density (assumed -5% in neutronic calculation);
- Cladding density (structural materials) (assumed -5% in neutronic calculation);
- Coolant density (assumed -5% in neutronic calculation);

Therefore, related reactivity insertions are computed. Reactivity insertions are considered with respect to a standard system variation regarding operative conditions close to normal core configuration – namely full operating at full power. Each system modification is associated to a reactivity coefficient, normalized per unity variation. It is then related to temperature in terms of functional dependence. Provided effects superposition, every transient involving thermal feedback is then described adding contributions according to all previous reactivity effects – the latter being properly weighted through temperature variation.

Basically, point kinetic neutronic model assumes integral approach to neutron transport Boltzmann equations in phase space (Henry (1975)). Therefore separation of variables is accomplished, supposing flux shape as a constant and amplitude as a time-dependent function. Point kinetic model is an amplitude transport model regarding system as a whole. A coherent approach requires system lumped parameters – different from local evaluations.

Global reactivity insertion is then evaluated for every system modification and related effects are applied to all core transients. Present analysis yielded a quite satisfying compromise between design phase dynamic evaluation and thermal-hydraulic feedback estimations aimed at flow blockage enhanced study. Indeed flux shape is accordingly kept as constant, conversely local effects are considered as far as direct calculations are performed.

The effect of the reactivity insertion on the power is then evaluated by the implementation of the 6-groups point kinetic equations into the CFX code. This scheme opens the possibility of a future two-way coupling between codes and it is summarized in Figure 38.

Total power $P(t)$ is represented as an amplitude $A(t)$ and a normalization coefficient P_0, representative the reference power value. Equations are then solved for such an amplitude A(t) function as well as neutron precursor normalized concentrations $C_i(t)$.

Total reactivity inserted is modelled as multiple effects superposition, as follows in scheme depicted here in the following.

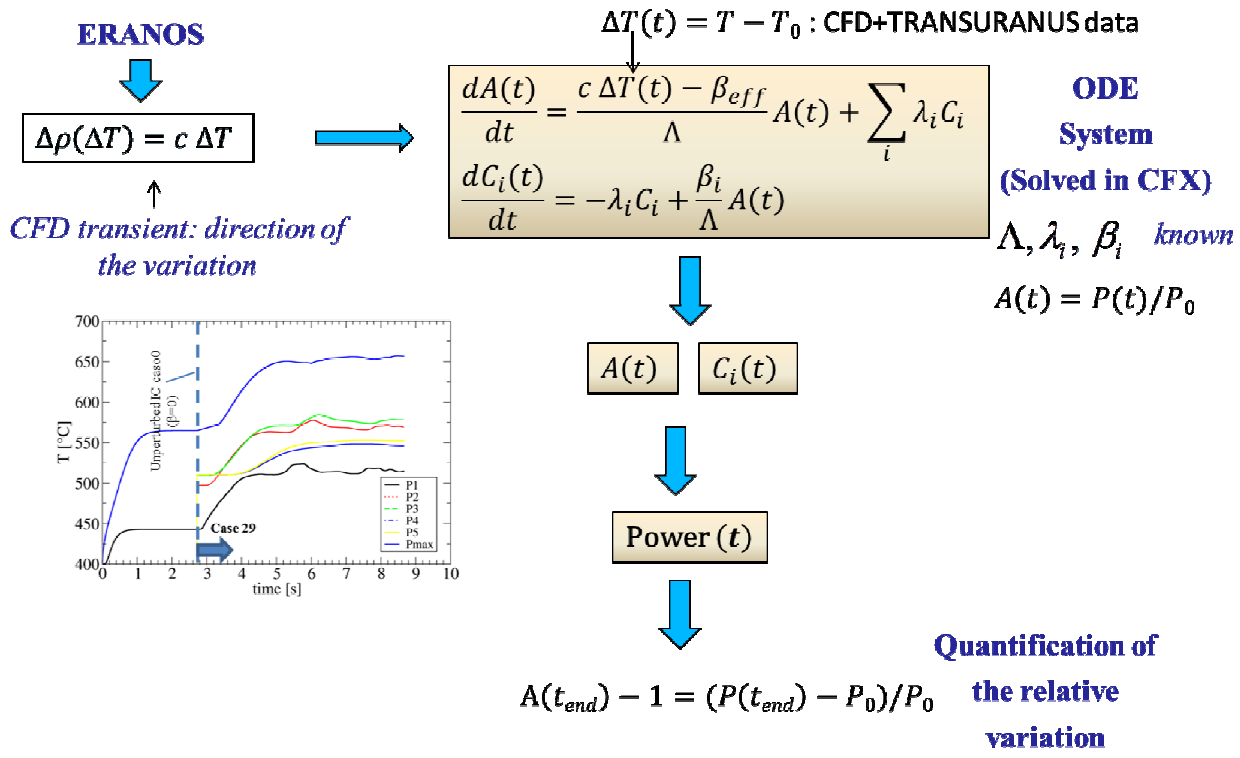

Figure 38 Schematic representation of the method used to quantify the neutronic feedback effect for the flow blockage.

In Table 10, c [pcm/K] represents the global neutronic feedback coefficient due to the temperature variation, $\Delta T(t)$ is the temperature variation during the transient, and $A(t)$ is the normalized power. Contribution $c\ \Delta T$ [pcm] represents the total reactivity insertion due to the blockage during the transient. Λ, λ_i, β_i are physical constants better defined in section 4.3, while C_i are the precursors groups populations.

Going in some details, the ERANOS code provides the feedback coefficients c_i with respect to previously listed: Doppler effect in the fuel, fuel density, coolant density, steel density and coolant void. The feedback coefficients and their meaning are summarized in Table 10.

Table 10 Feedback coefficients provided by the ERANOS code.

	Doppler	Fuel Density	Coolant Density	Steel Density
Name	c_1	c_2	c_3	c_4
Phys. Unit	[pcm/K]	[pcm/%density]	[pcm/%density]	[pcm/%density]

In our case, the coolant void coefficient is not of interest because the boiling of the lead during a blockage is virtually impossible due to the very high boiling temperature (T_{boil}~1700 °C). The density coefficients c_2, c_3, c_4 are here expressed with respect to the percentage variation of the density, i.e. they express numerically the reactivity insertion due to a positive variation of density of 1%.

The reactivity insertion due to the transient is then evaluated by multiplying coefficients times the relative variation of temperature or densities derived by the CFD simulation without feedback (in section 3).

All the contributions are then cumulated together in a total reactivity insertion $\Delta\rho_{tot}[pcm] = c_1 \cdot \Delta T_{fuel} + c_2 \cdot \Delta\hat{\rho}_{fuel} + c_3 \cdot \Delta\hat{\rho}_{coolant} + c_4 \cdot \Delta\hat{\rho}_{steel}$, where $\hat{\rho}$ is the density [kg /m^3].

This latter reactivity is now inserted as forcing term in the point kinetic equations solved by CFX multiplied by the normalized temperature variation in the transient:

$$\Delta\rho(t) = \Delta\rho_{tot} \cdot \frac{\Delta T(t)}{\Delta T_{\max}} \tag{1}$$

where total reactivity insertion $\Delta\rho_{tot}$ is referred to ERANOS simulation and $\Delta T_{\max}$ is the coherent temperature variation. According to previous, linear effects are superimposed for configurations close to nominal.

The output of the point kinetic calculation will thus be the normalized power function *A(t)* during the transient. Although this method is strictly one-way, it is conservative from an engineering point of view and it allows to quantify power variation during a flow blockage transient. Moreover, temperature profile is taken as an input and associated to feedback coefficients. Actually it comes from analysis in which no neutronic feedback were considered. According to results, neutronic feedback yield a global anti-reactivity insertion – namely a power reduction inside the core.

Previous analysis without neutronic effects turns out to be overestimated results about total power – being conservative as far as design needs are concerned. According to this, one-way coupling in accounting temperature profiles and time-dependent behaviour still provides an engineering and conservative characterization. Safety estimation of such a kind of accident - involving flow blockage - is thus achieved according to ongoing design phase and optimization.

Global current results highlight wide safety margins corresponding to this scenario, loosely impacting total core behaviour and dynamics.

4.2 ALFRED FA ERANOS Model

ALFRED core model considered within the framework of the present study is implemented according to design progress report (Petrovich (2013)). Main core parameters are as listed in table 11.

Table 11 Main core neutronic parameters for ERANOS code model implemented.

Core Power	300 MW_{th}
Core configuration	Hexagonal FA pattern
Inner Core Region	57 FA – 21.7% Pu enriched
Outer Core Region	114 FA – 27.8% Pu enriched

Fuel type	MOX fuel (U/Pu-O_2)
Control Rod Positions	12 FA (B_4C rods)
Safety Rod Positions	4 FA (B_4C rods)
Cladding material	1515Ti alloy
Active height	60 cm
Active radius	53 cm (8 annular hex slots)
Coolant/reflector	Liquid lead
Fuel burnup considered	Fresh (BOL)

Fuel assembly concerned by neutronic analysis is the central one - coherent with the thermal-hydraulic model. Material properties and operating conditions are resumed in table 12.

Table 12 Main core operating temperature parameters and material density.

Material	Density	Mean Temperature
Fuel (inner-outer)	10.49 g/cm3	900°C
Cladding (1515Ti)	7.95 g/cm3	460°C
Structural (T91)	7.73 g/cm3	460°C
Coolant (inlet)	11.01 g/cm3	400°C
Coolant (core midplane)	11.01 g/cm3	440°C
Coolant (outlet)	11.01 g/cm3	480°C

First, deterministic calculations were carried out starting from cell code ECCO which is a part of ERANOS 2.1 package. Computational domain is divided in several cells, both treated in homogeneous and in heterogeneous way. A cell is intended as a reactor region in which a particular neutron spectrum is present – dedicated neutronic calculations are performed.

Regions relevant to simulation concerning central channel are modelled as reported in Fig. 39.

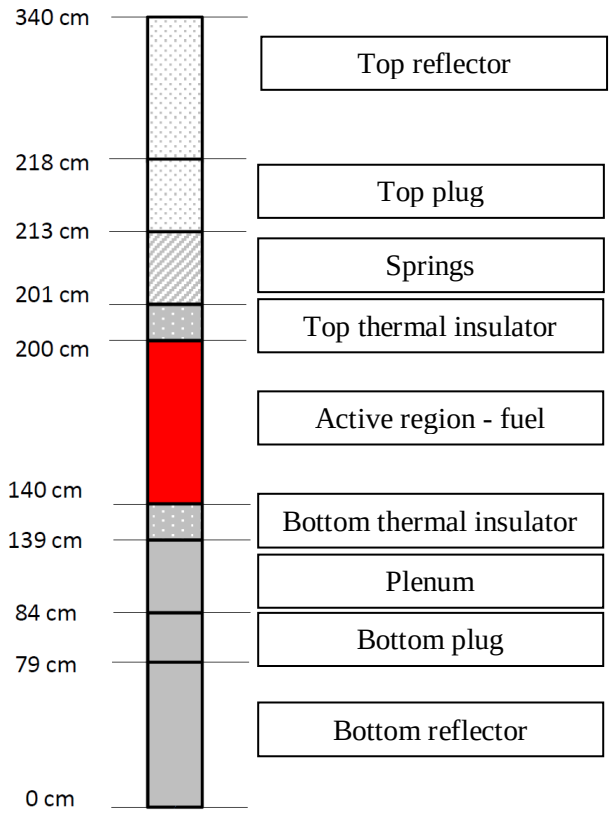

Figure 39 ERANOS model for neutronic calculation for cell code ECCO.

Cell description is either homogeneous or heterogeneous depending on impact of Doppler self-shielding and resonances in spectrum definition – regarding macroscopic cross-sections of the system. Nuclear data are processed by means of cell code ECCO. Areas are considered in heterogeneous fashion or in homogeneous one. Pin geometry – or particular frames - are implemented and FA lattice structure is considered. Nuclear data cross section calculations are carried out according to JEFF 3.1 nuclear data. Domain is treated at homogeneous level at 72 energy groups, P1 approximation thorough iterations approaching criticality – namely buckling imposed and self-shielding is evaluated. A second iteration is performed with 172 energy groups and heterogeneous domain. In addition, collision probability is used here accounting for an exact geometry. Energy structure is then extended to 1968 groups and all elements are treated for resonances. Energy structure is then condensed to 33 groups and finally homogeneous P1 data are stored for next reactor simulations. Previous calculation path is mainly retained for fuel region (inner and outer). Calculation cells description is provided in table 13.

Table 13 Main features for cell code ECCO, domain decomposition.

Cell Name	Domain Geometry	Principal Material	Main Composition
Bottom thermal insulator	FA pin lattice	Inside pin geometry	~100% Zr oxide
Top thermal insulator	FA pin lattice	Inside pin geometry	~100% Zr oxide
Spring	FA pin lattice	Inside pin geometry	~100% 1515Ti alloy
Plenum	FA pin lattice	Inside pin geometry	~100% 1515Ti alloy
Top plug	FA pin lattice	Inside pin geometry	85% 1515Ti – 15% Pb
Bottom plug	FA pin lattice	Inside pin geometry	90% 1515Ti – 10% Pb
Top reflector	Homogeneous	--	20% 1515Ti – 80% Pb
Bottom reflector	Homogeneous	--	12% 1515Ti – 88%

The Reactor core domain is then prepared. Hexagonal standard geometry is described through several annulus – size is coherent with CFD description reported. ERANOS standard nodal solver VARIANT is replaced with AVNM solver - which is similar to standards DSA methods for diffusion acceleration techniques of transport theory. Direct calculations are performed and core normal configuration is simulated – control rod positions are confirmed from technical design report as to approaching criticality (unity multiplication factor).

Simple variations are considered, regarding most impacting thermal-hydraulic perturbations occurring during the flow blockage transient – reported in table 14.

Table 14 Relevant parameter variations to be matched simulating flow blockage TH effects on neutronics.

Perturbation	Intensity Considered
Fuel Doppler broadening	$\Delta T = + 350°C$ (Ref. 950°C)
Fuel density	$\Delta\rho = -5\%$
Structural density	$\Delta\rho = -5\%$
Coolant density	$\Delta\rho = -5\%$

As previously explained, current method is based on local domain split. Actually, contribution are found by applying each perturbation to 12 axial slots of central channel. Results are obtained evaluating reactivity insertion related to every parameters change in all different slices accounting for local effect referred to total system integral parameter. The Active height (60 cm) is divided in 12 slots 5 cm height. This domain split was consistent to the calculation mesh decomposition and the method employed.

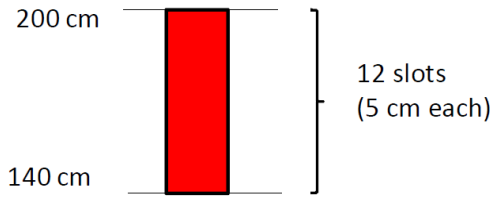

Figure 40 Active region central channel split for local axial profile for reactivity insertion.

Table 15 Axial reactivity coefficients profiles (central channel).

	Doppler (+350°C) [pcm]	Fuel Density (-5%) [pcm]	Coolant Density (-5%) [pcm]	Steel Density (-5%) [pcm]		Doppler (+350°C) [pcm]	Fuel Density (-5%) [pcm]	Coolant Density (-5%) [pcm]	Steel Density (-5%) [pcm]
Slot 1	-0.7	-8	-1.5	0.0	Slot 7	-0.4	-10	1.4	0.9
Slot 2	-0.6	-9	-0.1	0.4	Slot 8	-0.3	-9	1.0	0.8
Slot 3	-0.5	-10	1.0	0.7	Slot 9	-0.3	-7	0.5	0.6
Slot 4	-0.5	-11	1.8	1.0	Slot 10	-0.1	-6	-0.1	0.4
Slot 5	-0.5	-11	2.1	1.1	Slot 11	-0.1	-5	-0.9	0.1
Slot 6	-0.4	-11	1.9	1.1	Slot 12	-0.1	-4	-1.5	-0.1

Axial profiles for reactivity coefficient are then found and are reported in Table 15. Total amount is possibly computed for every single effect (fuel density, coolant density…) adding all axial contributions. Point kinetics is then implemented considering global superposition effects.

4.3 Power evaluation

To compute the neutronic feedback on the FA power in the case of blockage, the 6 groups point kinetic equations (Henry (1975)) were implemented in the ANSYS CFX 15:

$$\frac{dA(t)}{dt} = \frac{\Delta\rho(t) - \beta_{eff}}{\Lambda} \cdot A(t) + \sum_{i=1}^{6} \lambda_i C_i \tag{2}$$

$$\frac{dC_i(t)}{dt} = -\lambda_i C_i + \frac{\beta_i}{\Lambda} \cdot A(t) \tag{3}$$

where $A(t)$ is the dimensionless normalized power, $\Delta\rho(t)$ is the reactivity inserted (forcing term), C_i is the ith populations of precursors, λ_i is the decay constant of the ith precursor group, β_i is the fraction of all fission neutrons emitted that appear from the ith precursor group, $\beta_{eff} = \sum \beta_i$ is the total fraction of fission neutrons which are delayed, Λ is the prompt neutron lifetime. This nuclear parameters

depend on the fuel composition and on the energy or shape of the neutron spectrum, and therefore different numbers must be fixed for thermal and fast reactors and for the different fuels. In the case of the ALFRED fast reactor, the values of the parameters are summarized in Table 16 (NEA/WPEC-6 (2001)).

Table 16 Nuclear parameters relative to the point kinetic equations in the ALFRED reactor.

Λ [s]	$7.19 \cdot 10^{-7}$
β_1 [pcm]	11.6
β_2 [pcm]	101
β_3 [pcm]	71.5
β_4 [pcm]	110
β_5 [pcm]	28.8
β_6 [pcm]	15
β_{eff} [pcm]	338
λ_1 [1/s]	0.01247
λ_2 [1/s]	0.0305
λ_3 [1/s]	0.1114
λ_4 [1/s]	0.3014
λ_5 [1/s]	1.1363
λ_6 [1/s]	3.0137

Additional variables and equations were defined within CFX to represent the point kinetic equations system (Eqs. 2 and 3). The system of equations was integrated in time by using the CFX solvers.

To test the method, a simplified version of the point reactor kinetic equations with 1 group was implemented for which analytical solution yields:

$$\frac{dA(t)}{dt} = \frac{\Delta\rho(t) - \beta_{eff}}{\Lambda} \cdot A(t) + \lambda C \tag{4}$$

$$\frac{dC(t)}{dt} = -\lambda C + \frac{\beta_{eff}}{\Lambda} \cdot A(t) \tag{5}$$

Two test cases, namely C01 and C02, were solved for negative and positive reactivity insertion with the parameters in Table 17, representative of a typical thermal reactor.

Table 17 Parameters for 1-group point kinetic test cases C01 and C02.

	C01	C02
Λ [s]	10^{-3}	10^{-3}
β_{eff} [pcm]	750	750
λ [1/s]	0.08	0.08
$\Delta\rho$ [pcm]	250	-250

Results in terms of *A(t)* are presented in Figure 41. The numerical results are very close to the analytical solutions both for positive and negative reactivity insertion.

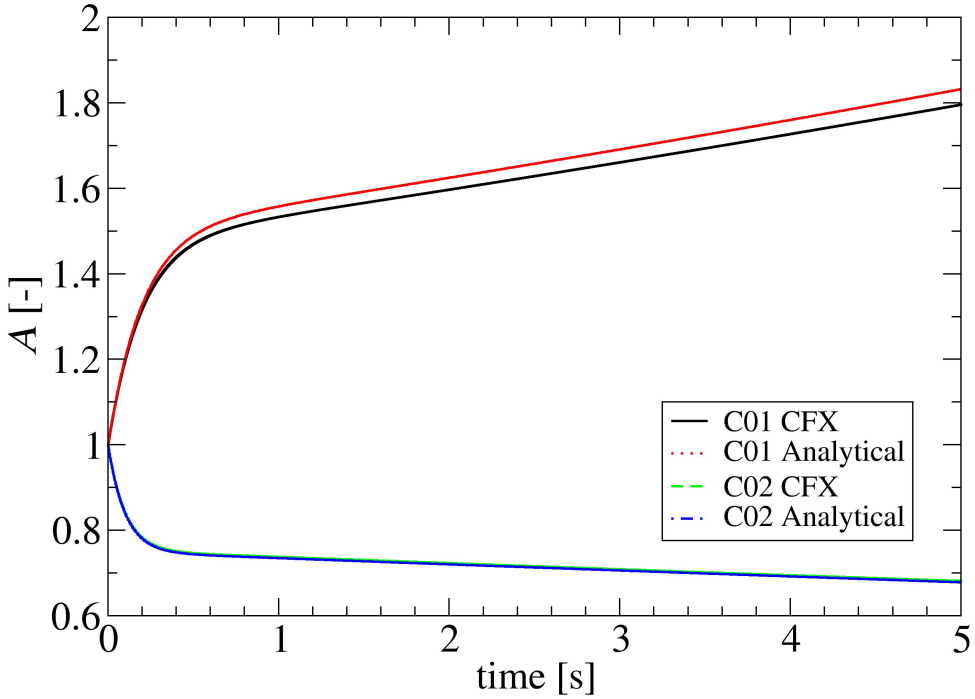

Figure 41 Comparison between CFX and analytical solutions for C01 and C02.

After this validation, the full system of 6 equations were integrated for the ALFRED reactor in case of blockage. The reference case chosen for the evaluation is case 30 in **Table 7**, i.e. a central blockage with 15% of the flow area blocked. The reactivity insertion can be deduced by the ERANOS coefficients according to a conservative fuel density variation of about 1%. Actually, coefficients c_1, c_2 and c_4 are too small to give a significant reactivity insertion during the transient. The only relevant contribution is due to the density variation of the fuel. This result is important and provides useful information on the neutronic feedback behaviour in case of different transients. If conservatively, 1% of variation in fuel density is assumed, about -20 pcm are introduced in the FA due to the flow blockage transient. The integration of the point kinetics with this forcing term, leads to the normalized power behaviour shown in Figure 42. In 10 s of transient, a variation of power around 10% can be assessed conservatively. According to these numbers, it is clear that the neutronic feedback in the case

of blockage can be considered as slightly impacting the design as far as safety calculations are concerned.

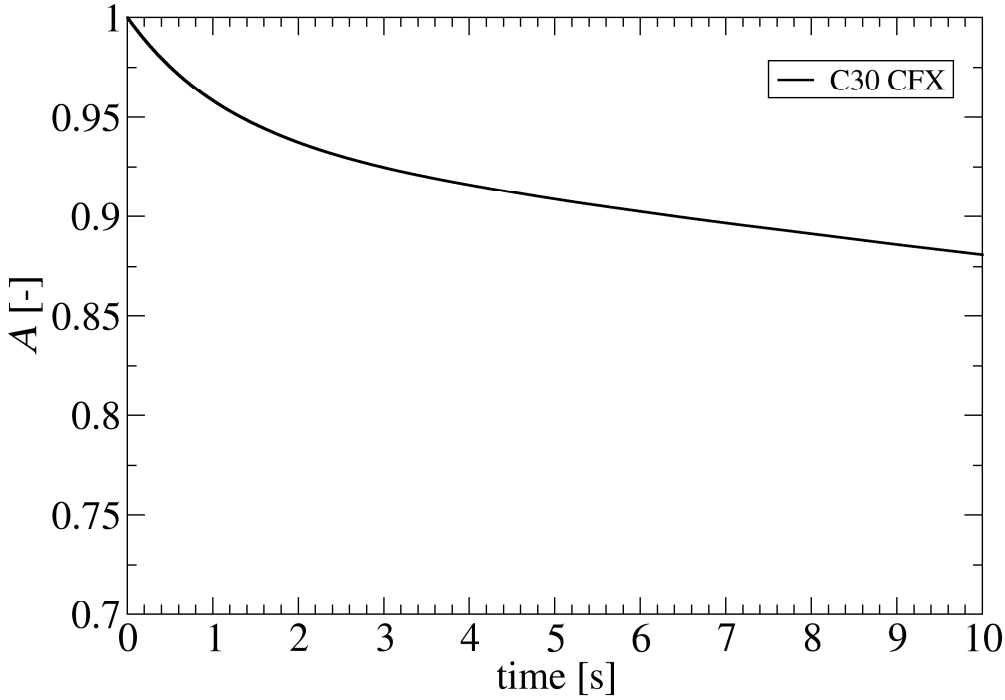

Figure 42 Solutions of 6-groups point kinetics with CFX for case 30 (15% blockage).

5. Conclusions

A CFD analysis by fully resolved RANS simulations was carried on fluid flow and heat transfer in the case of flow blockage in heavy liquid metal cooled fuel assemblies. The hexagonal closed ALFRED FA were considered for the study. The model includes the different FA regions (entry, active, follower, plenum), the conjugate heat transfer in the clad and the wrap, the bypass and power released by gamma. All the pins of the FA were modelled and no special symmetry planes were considered.

The reactivity feedback due to the temperature variation in the domain has not been considered. A constant power distribution was considered, neglecting the axial power profile, considered a second order effect at this stage. The study was carried with slightly overloaded conditions (wall heat flux q_{wall}=1 MW/m^2, against q_{wall}=0.69 MW/m^2 for an average pin and q_{wall}=0.93 MW/m^2 for a peak power pin) to be conservative from an engineering point of view.

Two main effects can be distinguished in a flow blockage: a local effect in the wake/recirculation region downstream the blockage and a global effect due to the lower mass flow rate in the blocked subchannels; the former (local) effect gives rise to a temperature peak behind the blockage and it is dominant for large blockages (β>0.2), while the latter (global) effect determines a temperature peak at the end of the active region and it is dominant for small blockages (β<0.1).

The blockage area was placed at the beginning of the active region, so that both over-mentioned phenomena can fully take place. The mass flow rate at the different degree of blockage was imposed from preliminary system code simulations.

Results indicate that a blockage of ~15% (in terms of area) leads to a maximum clad temperature around 800 °C, and this condition is reached in a characteristic time of 3-4 *s* without overshoot. The accident can be detected in the outlet section of the FA after 1 *s*. Local clad temperatures around 1000 °C can be reached for blockages of 30% or more.

A first evaluation of the neutronic feedback is given. The quantification is performed by a one-way coupling of the neutronic deterministic code ERANOS and the CFD code CFX.

Feedback coefficients are computed according to a central channel axial split and local effects are used through a lumped analysis, i.e. point kinetic model. The reactivity insertion is then obtained by superposition of significant parameters. Calculations indicate that relevant contribution to the overall reactivity comes from the fuel density variation, the latter being about -20 pcm. In the procedure, the temperature profile for reactivity insertion was assumed not influenced by the neutronic feedback. This hypothesis is conservative from an engineering point of view.

Present analysis indicates that the influence of the neutronic feedback on the power is around 10% and therefore a preliminary safety evaluation provides results which support current fuel assembly design.

6. Nomenclature

A	Section area [m^2]
c	Empirical constant
c_p	Specific heat at constant pressure [J/kgK]
d	Rod diameter [mm]
D_{eq}	Equivalent diameter [mm]
h	Heat transfer coefficient [MW/m^2K]
k	Thermal conductivity [W/mK]
L	Active length [m]
Nu	Nusselt number
p	Pitch [mm]
Δp	Pressure drop [Pa]
Pe	Peclet number
Pr	Prandtl number
q	Heat flux [MW/m^2]
Q	Total thermal power [MW]
Re	Reynolds number
R_{bl}	Blockage radius [mm]
T	Temperature [K]
w	Axial velocity [m/s]
w_0	Reference axial velocity [m/s]
z	Axial distance [mm]

Subscripts

$()_{clad}$	Clad
$()_{eff}$	Effective
$()_{inlet}$	Inlet
$()_{IO}$	Inlet-outlet
$()_{outlet}$	Outlet
$()_t$	Turbulent
$()_{wall}$	Wall

Greek Symbols

α	Thermal expansion coefficient [$1/K$]
β	Flow blockage area fraction
μ	Dynamic viscosity [$Pa \cdot s$]
μ_t	Eddy viscosity [$Pa \cdot s$]
ν	Kinematic viscosity [m^2/s]
ρ	Density [kg/m^3]
Θ	Non-dimensional temperature
Γ	Thermal diffusivity [m^2/s]

7. References

ANSYS CFX Release 13 User Manual, 2011.

Bandini, G., Bubelis, E., Schikorr, M., Stempnievicz, M.H., Lazaro, A., Tucek, K., Kudinov, P., Kööp, K., Jeltsov, M., Mansani, L., 2013. Safety Analysis Results of representative DEC accidental transients for the ALFRED reactor, IAEA-CN-199/260, 2013.

Bandini, G., 2014. Private communication.

Bertini, H.W., 1980. Description of selected accidents that have occurred at nuclear reactor facilities, ORNL/NSIC-176.

Chang, W.P., Ha, K.S., Suk, S.D., Jeong, H.Y., 2011. A comparative study of the MATRA-LMR-FB calculation with the SABRE result for the flow blockage accident in the sodium cooled fast reactor, Nucl. Eng. Des. 241, 5225-5237.

Cheng, X., Tak, N.I., 2006. CFD analysis of thermal-hydraulic behavior of heavy liquid metals in sub-channels, Nucl. Eng. Des. 236, 1874-1885.

Di Piazza, I., Scarpa, M., Tarantino, M., 2013. A CFD analysis of convective heat transfer in the ice fuel pin simulator, *submitted* to Nucl. Eng. Des.

Di Piazza, I., Magugliani, F., Tarantino, M., Alemberti, A., 2014. A CFD analysis of flow blockage phenomena in ALFRED LFR demo fuel assembly, Nucl. Eng. Des. 276, 202-215.

Han, J.T., Fontana, M.H., 1977. Blockages in LMFBR Fuel Assemblies – A Review. Proc. Winter Annual ASME meeting.

Hooper, J.D., Wood, D.H., 1982. Flow Recovery from a Single Subchannel Blockage in a Square-Pitched Rod Array. Nucl. Eng. Des. 74, 91-103.

Klein, G.A., Sesonske, A., 1981. Heat Transport and Recirculating Flow Distribution Behind a Normal Blockage, with Application to LMFBRS. Nucl. Eng. Des. 68, 385-395.

Kirsch, D., 1973. Investigation on the Flow Temperature Distribution Downstream of Local Coolant Blockages in Rod Bundle Subassemblies, Nucl. Eng. Des. 31, 266-279.

Lu, Q., Qiu, S., Su, G.H., Flow Blockage Analysis of a channel in a a typical material test reactor core. Nucl. Eng. Des. 239, 45-50.

Maity, R.K., Velusamy, K., Selvaraj, P., Chellapandi, P., 2011. Computational fluid dynamic investigations of partial blockage detection by core-temperature monitoring system of a sodium cooled fast reactor. Nucl. Eng. Des. 241, 4994-5008.

Mansani, L., 2013. Private communication.

Menter, F. R., 1994.Two-equation eddy-viscosity turbulence models for engineering applications. AIAA J. 32, 269-289.

NRC "Fermi, Unit 1", NRC Website, 3 February 2011, accessed 17 March 2011.

OECD/NEA, 2007. Handbook on Lead-bismuth Eutectic Alloy and Lead Properties, Materials Compatibility, Thermal-hydraulics and Technologies, NEA No. 6195.

RCC-MRx, 2010. Design and Construction Rules for mechanical components of nuclear installations, ed.AFCEN.

Rimpault, G., 2002. The ERANOS code and data system for fast reactor neutronic analyses, International Conference on the PHYsics Of Reactors (PHYSOR 2002), Seoul, Korea.

Scarpa, M., 2013. CFD Thermal Hydraulic Analysis of HLM cooled rod bundles, *Master Thesis* Univ. of Pisa, Italy.

Schultheiss, G.F., 1987. On local blockage formation in sodium cooled reactors. Nucl. Eng. Des. 100, 427-433.

Warden, J.M., Mount, M., Lynn, N.M.. Possible Criticalities of the Marine Reactors Dumped in the Kara Sea. Proc. 3rd International conference on the radioactivity in the arctic, Thomso, Norway, June 1-5, 1997.

Zrodnikov, A.V., Chitaykin, V.I., Gromov, B.F., Grigoryv, O.G., Dedoul, A.V., Toshinski, G.I., Dragunov, Y.G., Stepanov, V.S.. Use of Russian Technology of ship reactors with lead-bismuth coolant in nuclear power. *Russian Federation Report* XA0056274, 2000.

Qing Lu et al., 2009, Flow blockage analysis of a channel in a typical material test reactor core, Nucl. Eng. Des., 239, 45-50.

M. Adorni et al., 2005, Analysis of partial and total flow blockage of a single fuel assembly of an MTR research reactor core, Ann. Nuc. En., 32, 1679-1692

X.J. Liu et al., 2013, Thermal-hydraulic analysis of flow blockage in a supercritical water-cooled fuel bundle with sub-channel code, Ann. Nuc. En., 59, 194-203

S. Jewer at al., 2014, An immersed body method for coupled neutron transport and thermal hydraulic simulations of PWR assemblies, Ann. Nuc. En., 68, 124-135

Hyung Min Son et al., 2015, Flow blockage accident or loss of flow accident by using comparative approach of NK/TH coupling codes and RELAP5 code, Ann. Nuc. En., 64, 311-319Hyung Min Son et al., Transient thermal–hydraulic analysis of complete single channel blockage accident of generic 10 MW research reactor, Ann. Nuc. En., 75, 44-53

E. Ampomah-Amoakoe et al., 2013, CFD analysis of the dynamic behavior of a fuel rod sub-channel in a supercritical water reactor with point kinetics, Ann. Nuc. En., 39, 211-223

W.P. Chang et al., 2011, A comparative study of the MATRA-LMR-FB calculation with the SABRE result for the flow blockage accident in the sodium cooled fast reactor, Nucl. Eng. Des., 241, 5225-5237C. Petrovich, ALFRED core. Summary, synoptic tables, conclusions and recommendations, Technical Report PAR Research Program, ENEA UTIFISSM-P9SZ-006, 2013

A.F. Henry, Nuclear Reactor Analysis, MIT University Press, 1975

Delayed Neutron Data for the Major Actinides, NEA/WPEC-6, OECD 2002